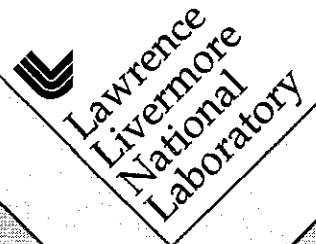


KARAB Containment Data Report

T. Stubbs
R. Heinle

July 1998



This is an informal report intended primarily for internal or limited external distribution. The opinions and conclusions stated are those of the author and may or may not be those of the Laboratory.

Work performed under the auspices of the U.S. Department of Energy by the Lawrence Livermore National Laboratory under Contract W-7405-ENG-48.

DISCLAIMER

This document was prepared as an account of work sponsored by an agency of the United States Government. Neither the United States Government nor the University of California nor any of their employees, makes any warranty, express or implied, or assumes any legal liability or responsibility for the accuracy, completeness, or usefulness of any information, apparatus, product, or process disclosed, or represents that its use would not infringe privately owned rights. Reference herein to any specific commercial products, process, or service by trade name, trademark, manufacturer, or otherwise, does not necessarily constitute or imply its endorsement, recommendation, or favoring by the United States Government or the University of California. The views and opinions of authors expressed herein do not necessarily state or reflect those of the United States Government or the University of California, and shall not be used for advertising or product endorsement purposes.

This report has been reproduced
directly from the best available copy.

Available to DOE and DOE contractors from the
Office of Scientific and Technical Information
P.O. Box 62, Oak Ridge, TN 37831
Prices available from (615) 576-8401, FTS 626-8401

Available to the public from the
National Technical Information Service
U.S. Department of Commerce
5285 Port Royal Road
Springfield, VA 22161

KARAB Instrumentation Summary

Instrumentation	Fielded on this Event	Data Return	Present in this Report
<u>Plug Emplacement</u>	yes	yes	yes ^(a)
<u>Radiation</u>	yes	yes	yes
<u>Pressure</u>			
Stemming	yes	yes	yes
Challenge	no	-	-
Cavity	no	-	-
Atmospheric	no	-	-
<u>Motion</u>			
Free Field	yes	yes	yes
Surface	yes	yes	yes
Plug	no	-	-
Stemming	no	-	-
Surface Casing	no	-	-
Emplacement Pipe	no	-	-
<u>Hydroyield</u>	no	-	-
<u>Collapse</u> ^(b)	yes	yes	yes
<u>Stress</u>	yes	yes	no
<u>Strain</u> ^(c)	yes	yes	no
<u>Other Measurements</u>	no	-	-

- (a) Description only.
(b) EXCOR or CLIPER in emplacement and satellite holes.
(c) Strain load on emplacement pipe.

Event Personnel

Containment Physics		Instrumentation	
B. Hudson	LLNL	L. Starrh	LLNL
F. Morrison	LLNL	D. Lonneaux	EG&G/AVO
J. Kalinowski	EG&G/AVO	W. Webb	EG&G/NVO
T. Stubbs	EG&G/AVO	A. Moeller	EG&G/NVO

Contents

1.	Event Description								
1.1	Site	1
1.2	Instrumentation	1
1.3	Emplacement	2
2.	Stemming Performance								
2.1	Pressure and Radiation	9
2.2	Motion	23
3.	Collapse Phenomena	
3.1	Pressure and Radiation	38
3.2	Motion	38
	References	54

1. Event Description

1.1 Site

The KARAB event was detonated in hole U4ah of the Nevada Test Site as indicated in figure 1.1. The KARAB device had a depth-of-burial (DOB) of 331 m in the Tunnel Beds tuff of area 4, about 200 m above the Paleozoic formation and the standing water level, as shown in figure 1.2 ⁽¹⁾. Stemming of the 2.44 m diameter emplacement hole followed the plan shown in figure 1.3. Stemming design of the satellite hole Ue4ad, 14.9 m due East of the emplacement hole, is shown in figure 1.4. A log of the stemming operations was maintained by Holmes & Narver⁽²⁾.

Detonation time was 07:51 PST on March 16, 1978 and collapse progressed to the surface about 53 minutes after detonation. The resulting surface crater had an average radius of 60.3 m and a maximum depth of 7.6 m.

No radiation arrivals were detected above ground and containment of the KARAB event was considered successful.

1.2 Instrumentation

Figure 1.5 is a schematic layout of the instrumentation designed to monitor the emplacement procedures and stemming performance of the KARAB event.

Pressure and radiation were monitored at seven elevations (stations) in the stemming material of the emplacement hole, as shown in figure 1.5.

Vertical free-field motion was monitored at ten elevations (stations) in the satellite hole Ue4ad and the ground surface. Accompanying each of the motion stations, but about 4 m deeper than each, was a vertical stress gauge supplied by Sandia Corp. See figure 1.6. The signals recorded from the stress transducers were without calibration information and appeared to lack information of any kind; they are not reported here.

Signals from each of the above instruments were transmitted to the recording trailer by an analog system and recorded on magnetic tape.

D-cables, used for quality assurance during the stemming operations, were also recorded post-shot. One CLIPER sensor was mounted in the emplacement hole on the containment gauge pendant along with the D-cable to monitor the progression of cavity collapse and one was fielded inside the emplacement pipe. Another pair of CLIPER's were fielded in the satellite hole.

Details of the instrumentation are given in reference 3.

1.3. Emplacement

Both stemming plugs above the KARAB event consisted of "LAE 59" rigid coal-tar epoxy (CTE) layers. The top plug was composed of a 2.0 m layer of rigid foam cubes and sand, sandwiched between layers of CTE. The total thickness of the two layers of CTE in the top plug was 7.0 m which was designed to be completely contained within the bottom portion of the surface casing, beginning about 4.5 m above the bottom of the casing.

Stemming between the plugs consisted of "LLL Stemming Mix", a graded sand and gravel mixture. The top 22 m of the hole (above the top plug) was also filled with LLL Stemming Mix. Stemming of the emplacement pipe consisted of plastic sealing material for about 0.5 m next to the diagnostics canister, followed by grout to a point about 4 m below the ground surface and topped off by another plastic sealing plug. See figure 1.3.

Instrumentation for the satellite hole was hung on a fiber glass pipe, oriented to the device, and then grouted from depth to the ground surface. See figure 1.6.

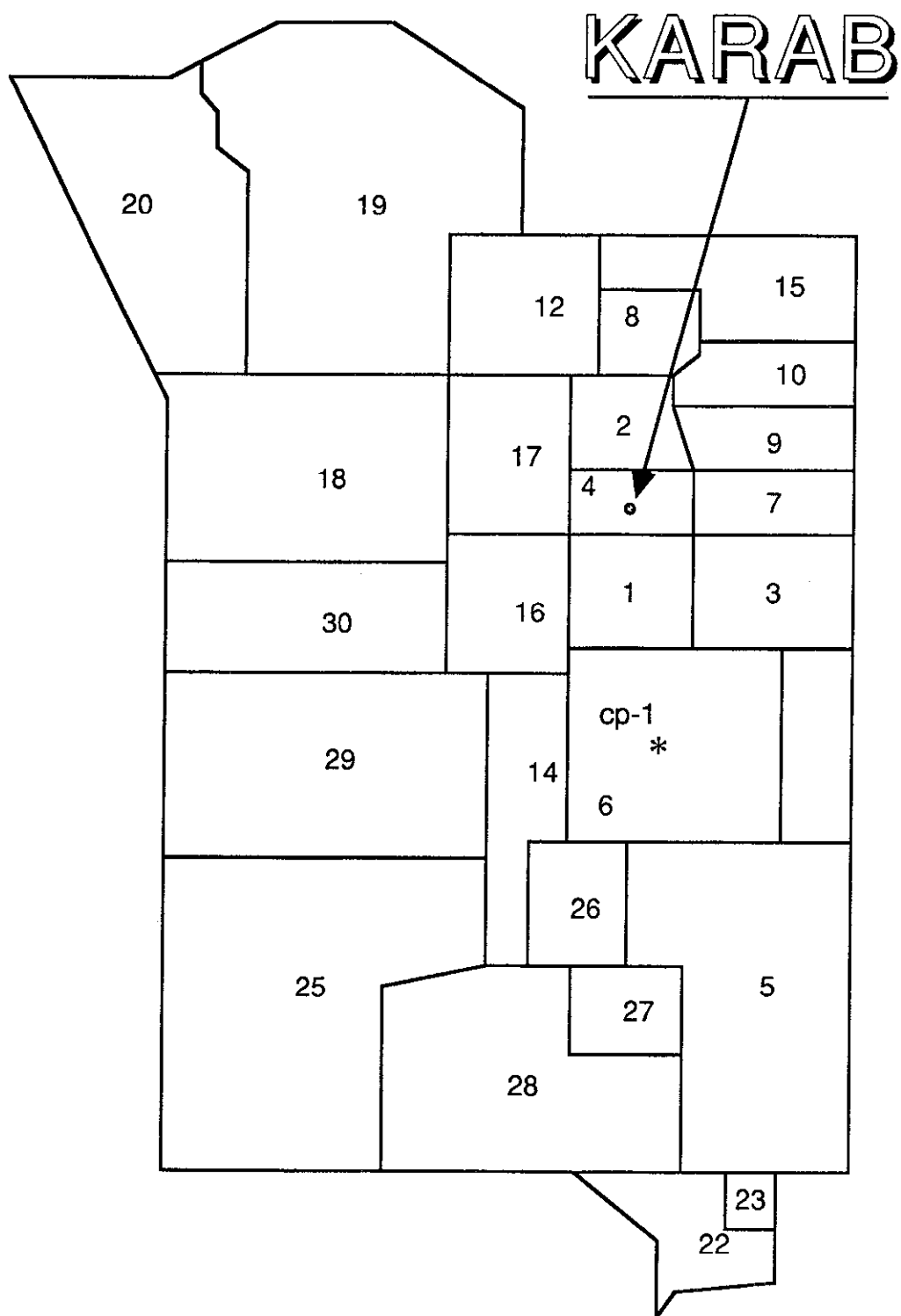


Figure 1.1 Map of the Nevada Test Site indicating the location of hole U4ah.

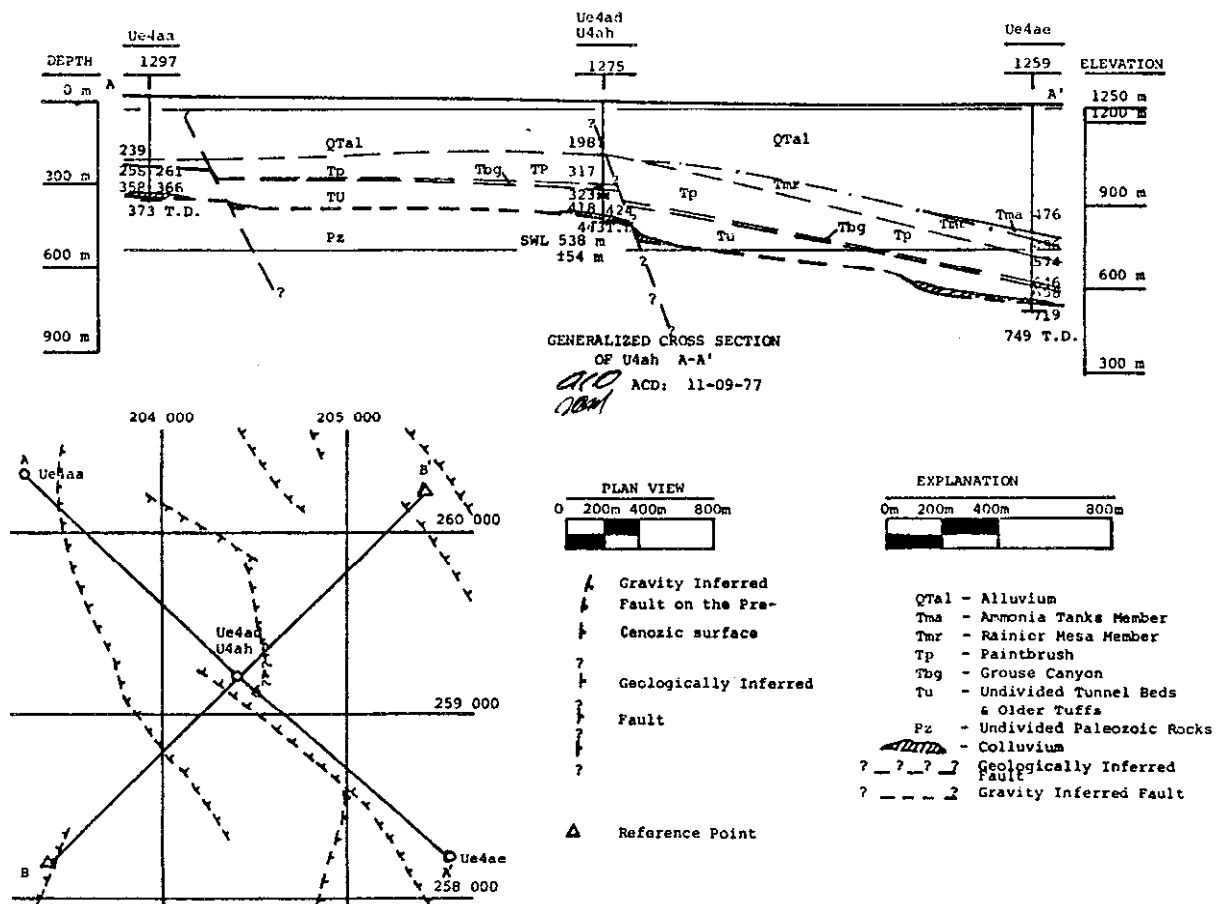


Figure 1.2 Northwest-southeast geologic cross section through hole U4ah including a plan map of the vicinity. Ue4ad is 114.9 m due East of U4ah.

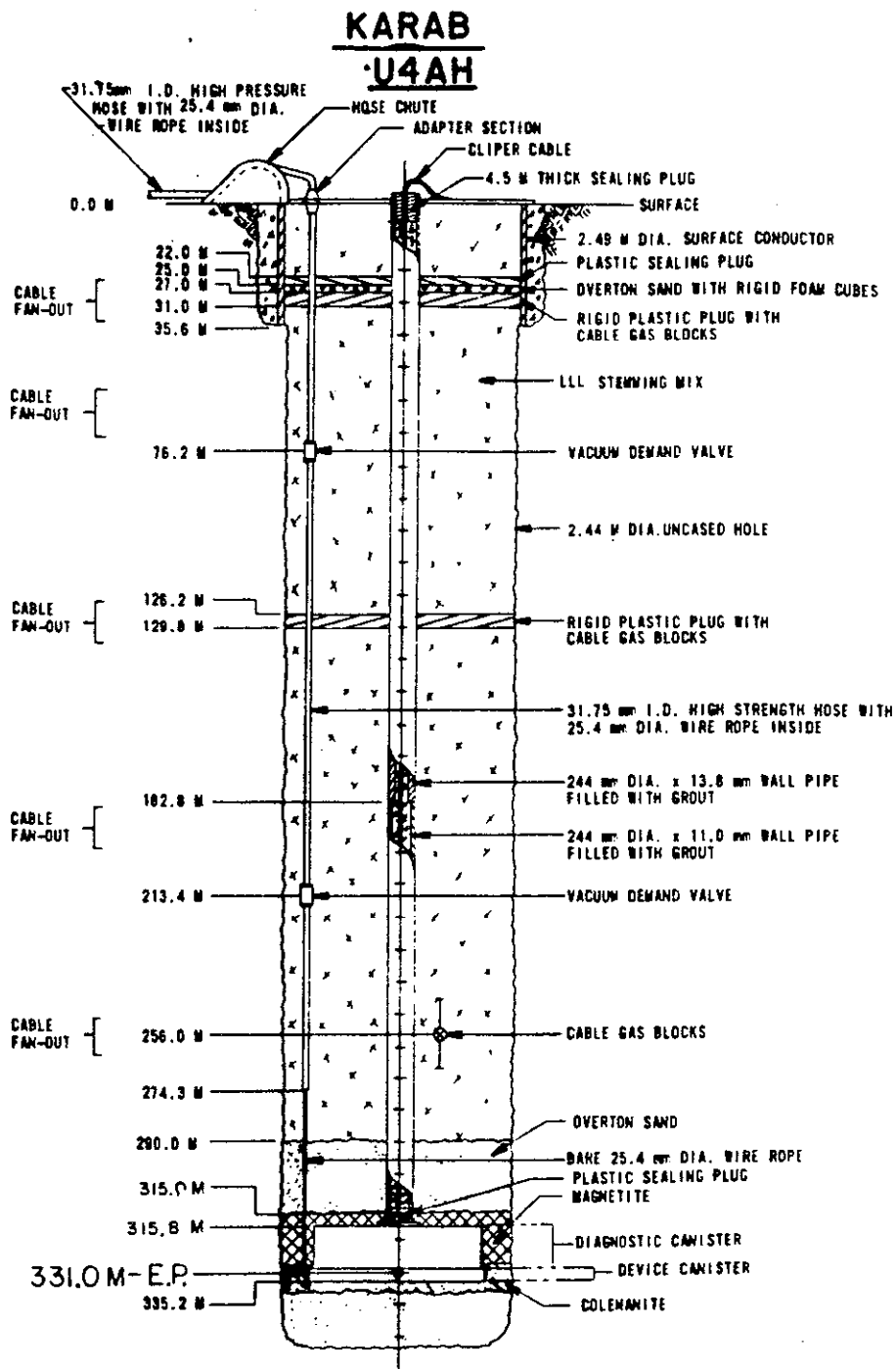


Figure 1.3 As-built stemming plan for the event KARAB in Hole U4ah.

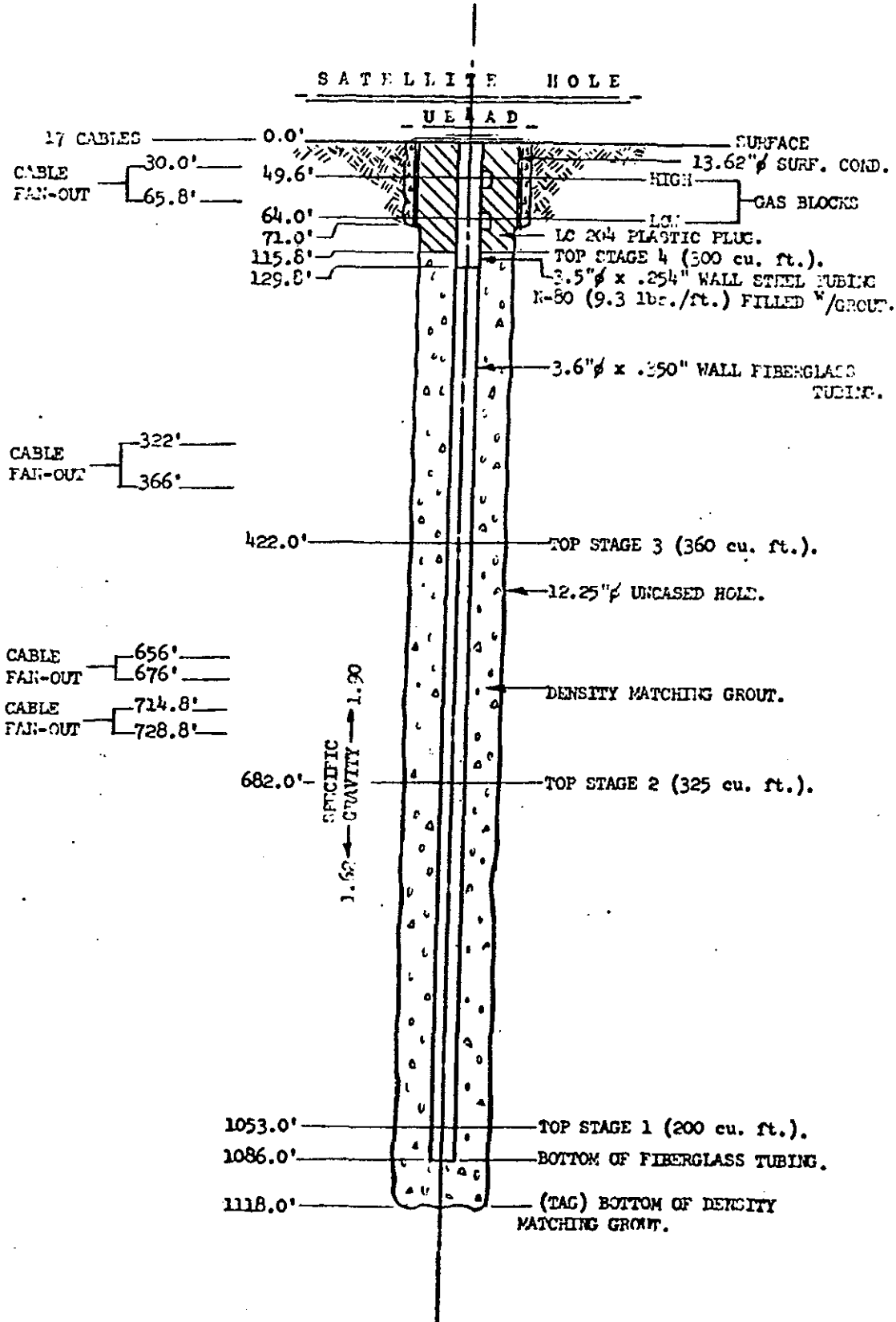
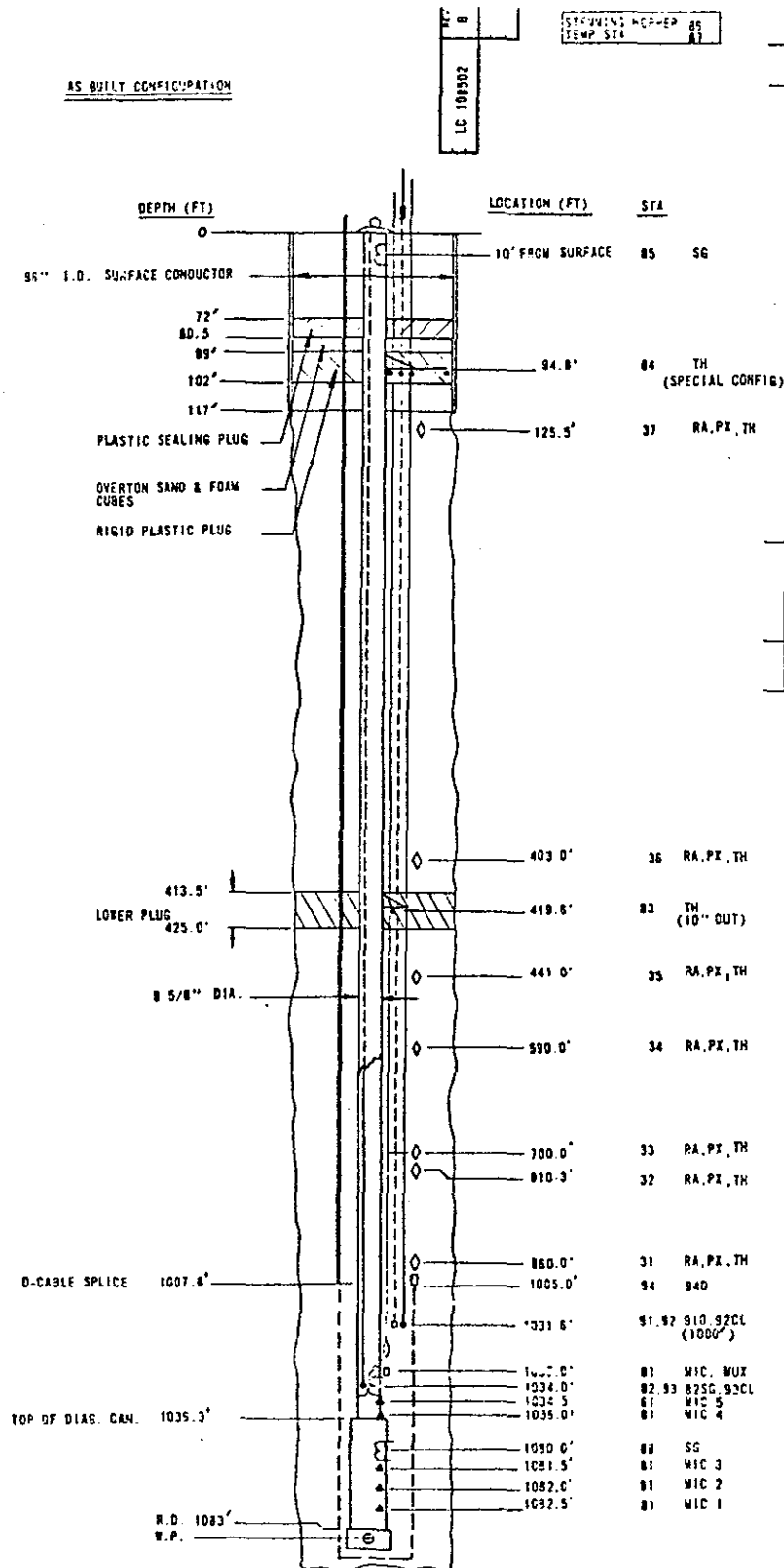


Figure 1.4 As-built stemming plan for the satellite Hole Ue4ad.

PART NO.		REVISION	
LC 108502		REVISED TO REFLECT "AS BUILT" CONDITION	
DATE	BY	DATE	BY
3/10/78	LC	3/10/78	LC
DESCRIPTION		DESCRIPTION	
REVISED TO REFLECT "AS BUILT" CONDITION		REVISED TO REFLECT "AS BUILT" CONDITION	



EG&G		P.O. BOX 200 SAN RAMON, CALIFORNIA 94583	
SPECIAL MEASUREMENTS		KARAB U4AH	
DATE	TIME	DATE	TIME
3/10/78	11:17:37	3/10/78	11:17:37
CHECKED	DESIGNED	ENGINEER	PROBLEM
MAHON	MAHON	D. Mahon	MAHON
LIST OF MATERIAL OR PART LIST		99626 C	
PART NO.		99626 C	
DESCRIPTION		99626 C	
LAST REVIEW USED		99626 C	
OUTGOING AND TOLERANCE PER		99626 C	
USAF 115		99626 C	
WELLS SHALL BE FULL STRENGTH OF		99626 C	
MATERIAL AND SHALL BE INSULATED		99626 C	
WITH AIR OR ALC STANDARDS		99626 C	
MACHINED SURFACES TO BE 12.5		99626 C	
UNLESS OTHERWISE SPECIFIED		99626 C	
DO NOT SCALE THIS DRAWING		99626 C	
LEGEND		99626 C	
◇ STEERING CANISTER		99626 C	
PX BACKFILL PRESSURE		99626 C	
TH THERMISTOR		99626 C	
△ THERMISTOR EMPLACEMENT		99626 C	
D CABLE		99626 C	
E STRAIN GAGE (SG)		99626 C	
▲ MICROPHONE (MIC)		99626 C	
□ MICROPHONE MULTIPLIER		99626 C	
(MIC MUX)		99626 C	
CLIPPER (CL)		99626 C	
V PENDANT		99626 C	
RA RADIATION MEASUREMENT		99626 C	

Figure 1.5 As-built containment instrumentation plan for the emplacement hole (U4ah) on the KARAB event.

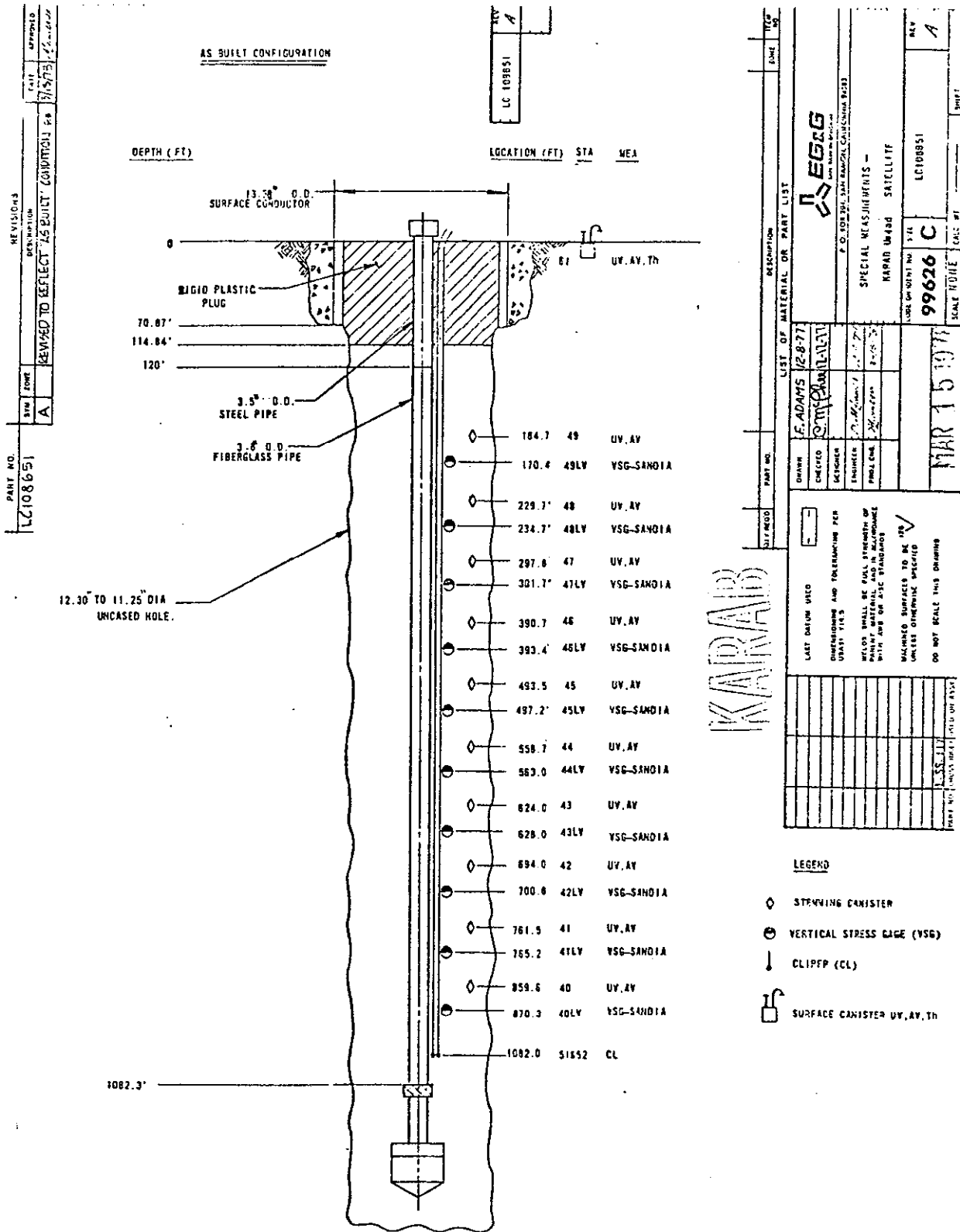


Figure 1.6 As-built instrumentation plan for the satellite hole (Ue4ad) on the KARAB event.

2. Stemming Performance

2.1 Pressure and Radiation

Pressure and radiation were monitored on the KARAB event at seven stations in the stemming of the emplacement hole and the early portions of the wave forms from these stations are shown in figures 2.1–2.7. Station 31 was lost shortly after 1 second (figure 2.1) and the radiation transducers at all the other stations (except station 34) exhibited the common loss of signal at zero time with recovery at some later time. Station 4 (figure 2.4) was lost close to zero time and the signals from it are shown for completeness. The entire pressure and radiation histories from 1 minute before detonation to such time as signals were lost due to collapse or when recording was terminated are shown in figures 2.8 – 2.13 (station 34 is omitted). Figure 2.8 (station 31) suggests that the pressure exceeded and remained above 60 psia, the system limit, beyond the collapse time of about 3200 s. This record should be disregarded. Station 37, just below the top plug and the surface casing, survived collapse. This was presumably due to the cable protection afforded by the surface casing.

The only radiation history detected is shown in figure 2.9. This was in the stemming about 83 m above the working point (station 32). All other stations indicate that there was no radiation at elevations above this prior to collapse when the station signals were lost. Station 37, which survived collapse, showed no radiation arrival at any time.

Pressure histories at stations 31 and 32 (figures 2.1 and 2.2) suggest an influence from the cavity gases while the pressure histories at all other stations can be explained as resulting from ground or stemming motion.

No radiation arrivals were observed above ground at any time after the KARAB event and the data are consistent with satisfactory containment.

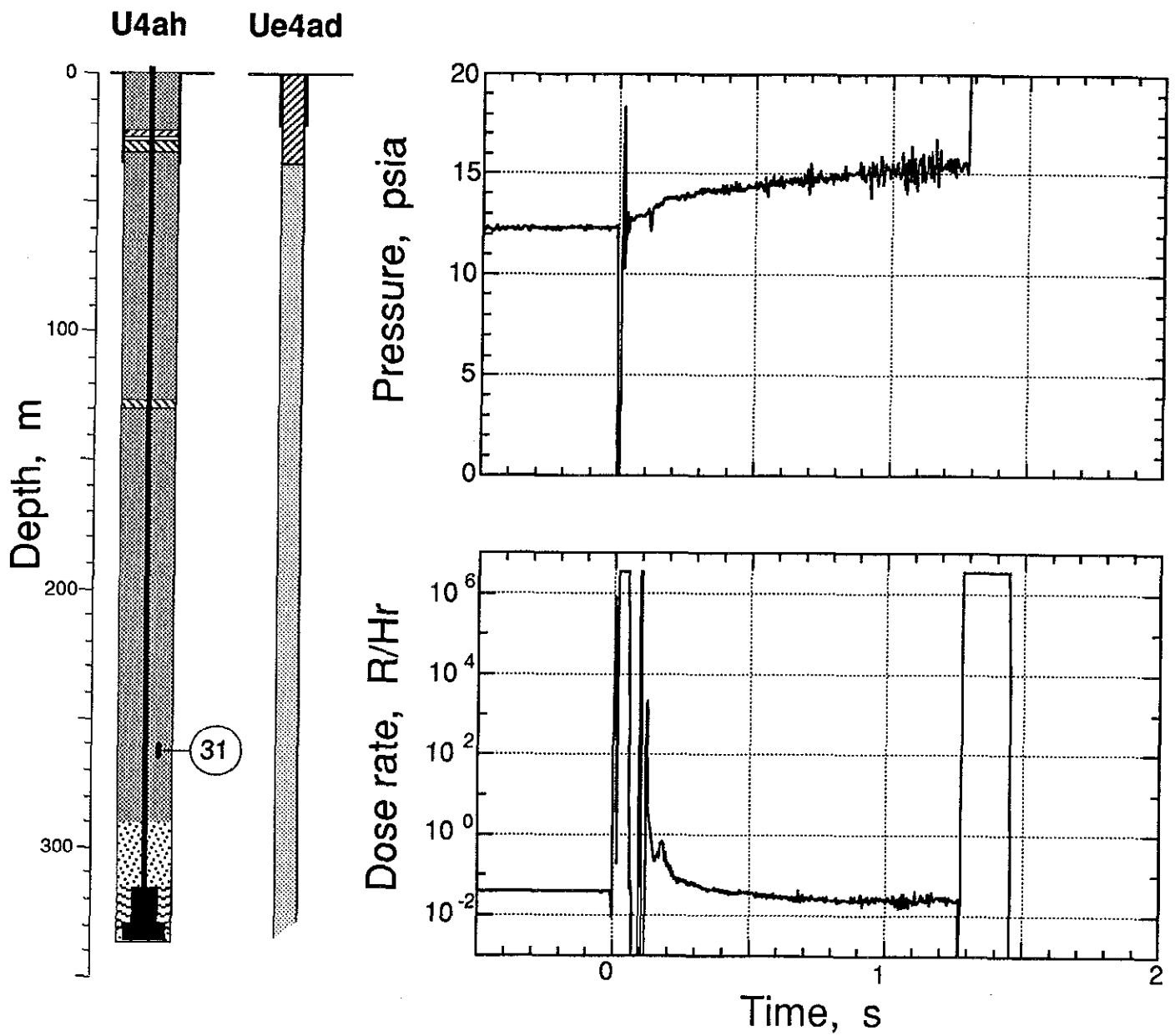


Figure 2.1 The first 2 s of pressure and radiation detected in the fines stemming of the emplacement hole (Station 31 at a depth of 262 m).

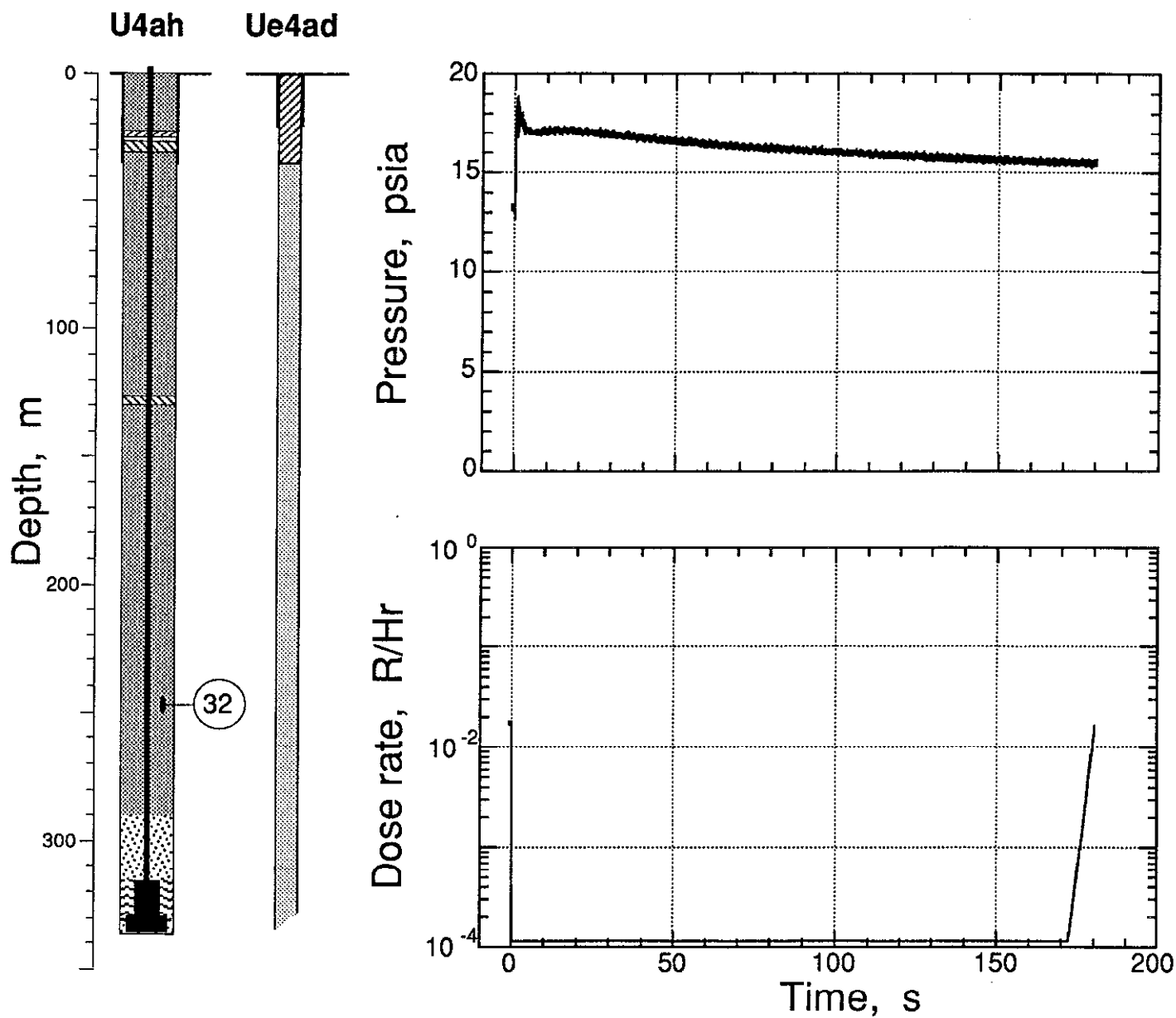


Figure 2.2 The first 200 s of pressure and radiation detected in the fines stemming of the emplacement hole (Station 32 at a depth of 247 m). The radiation transducer was saturated by the EMP and began to recover about 170 s later.

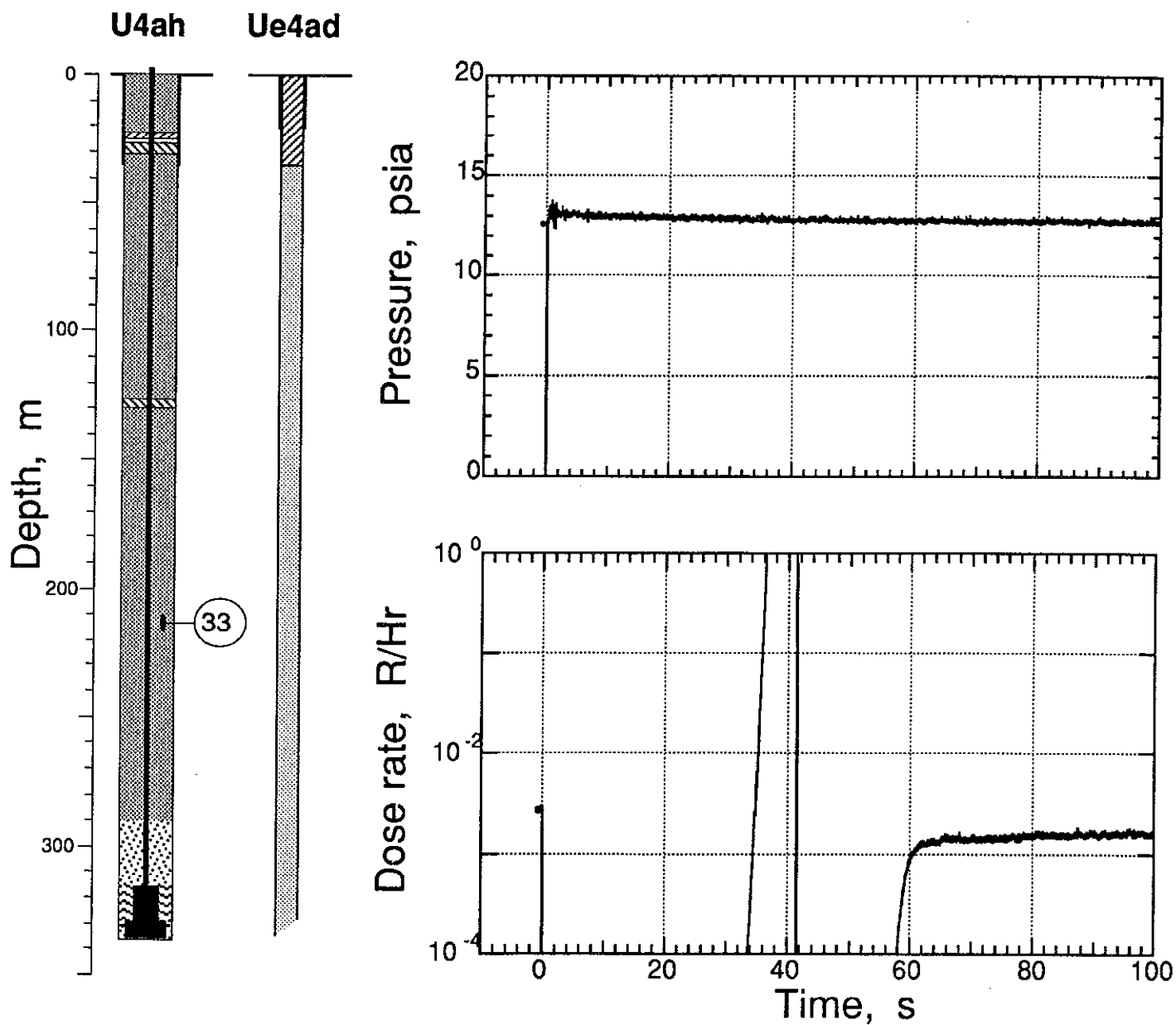


Figure 2.3 The first 100 s of pressure and radiation detected in the fines stemming of the emplacement hole (Station 33 at a depth of 213 m). The radiation transducer was saturated by the EMP and began to recover about 60 s later.

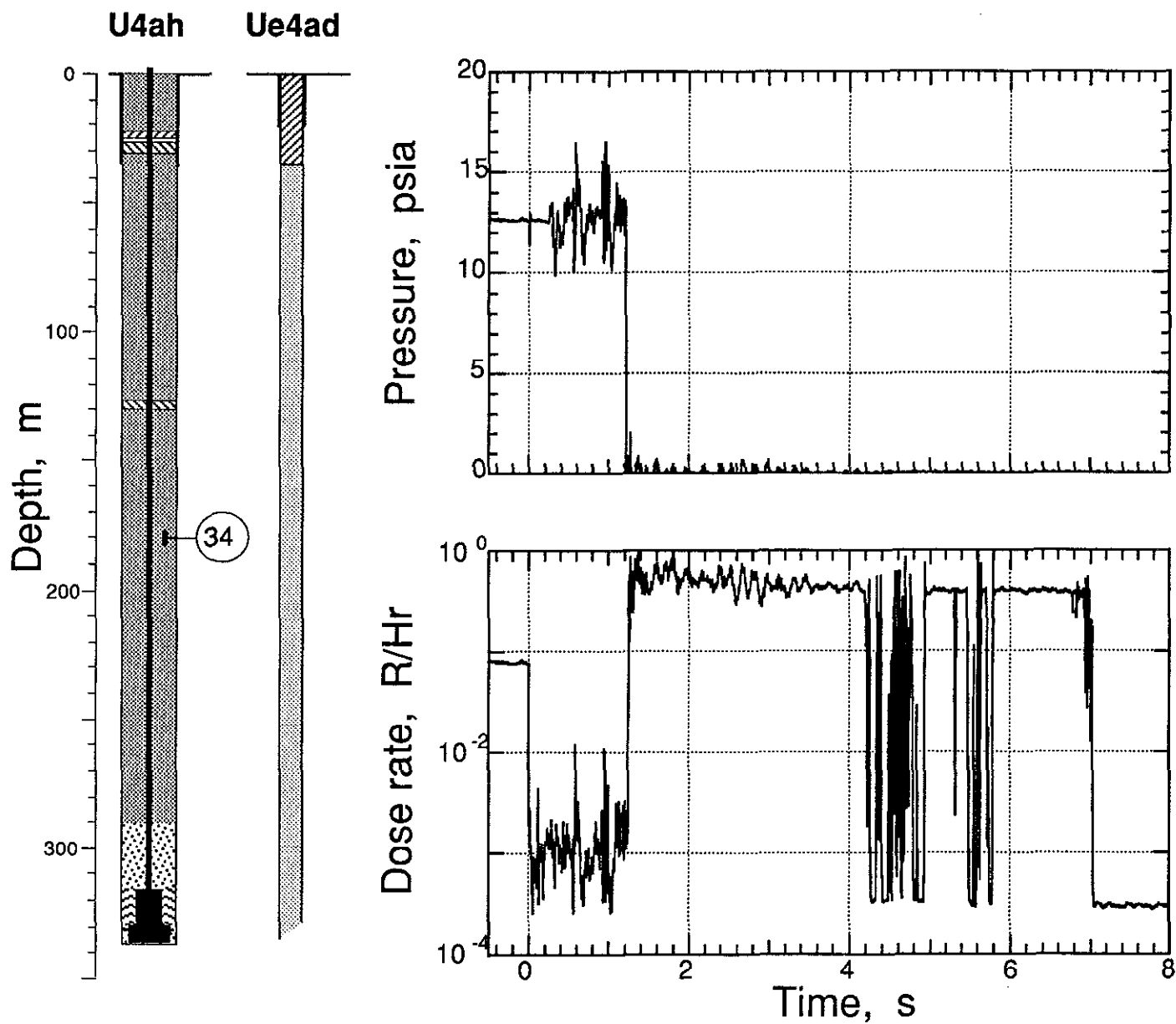


Figure 2.4 The first 8 s of pressure and radiation detected in the fines stemming of the emplacement hole (Station 34 at a depth of 180 m). This station was lost shortly after 1 second.

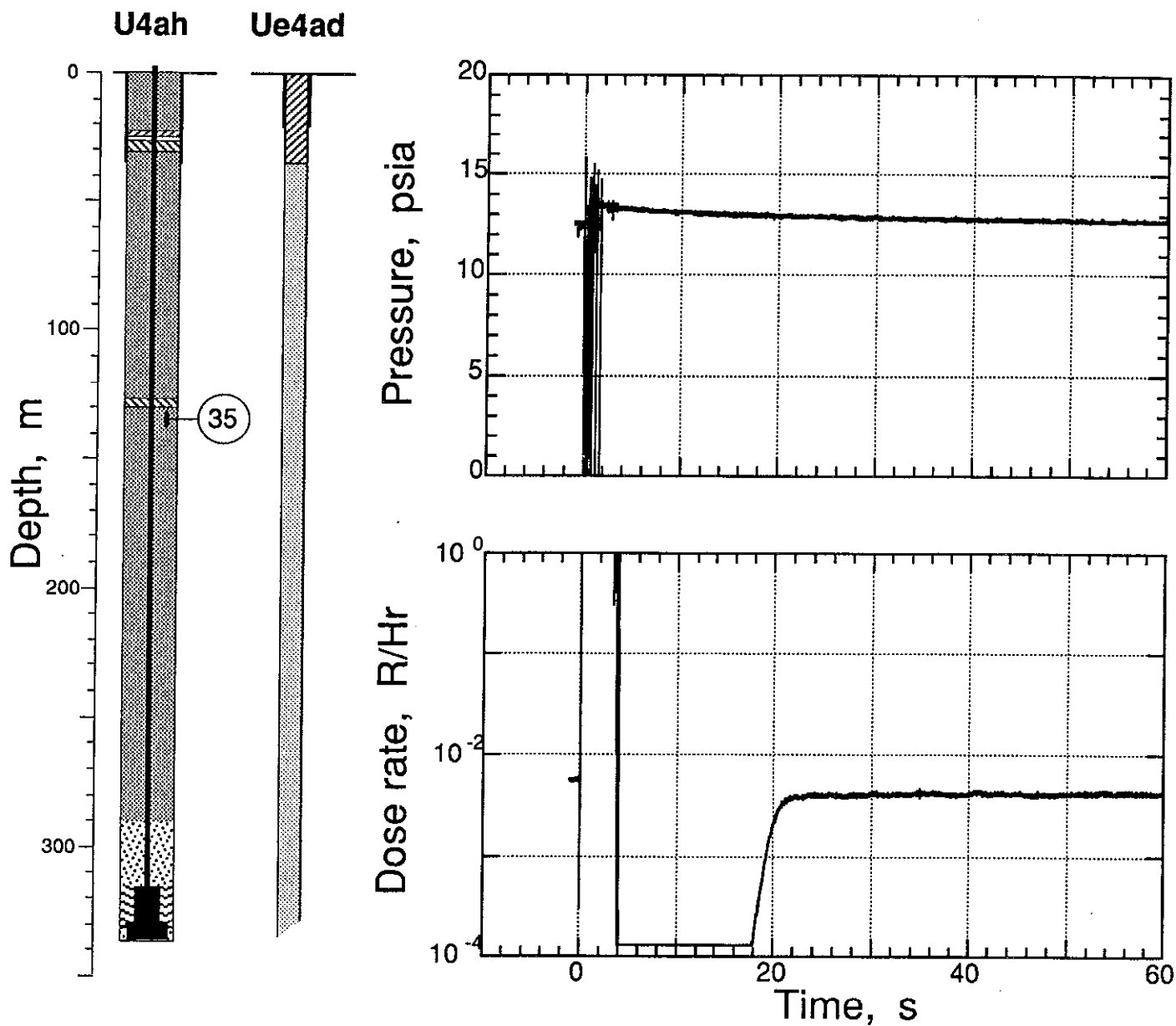


Figure 2.5 The first 60 s of pressure and radiation detected in the fines stemming of the emplacement hole below the rigid plug (Station 35 at a depth of 134 m). The radiation transducer was saturated by the EMP and began to recover about 20 s later.

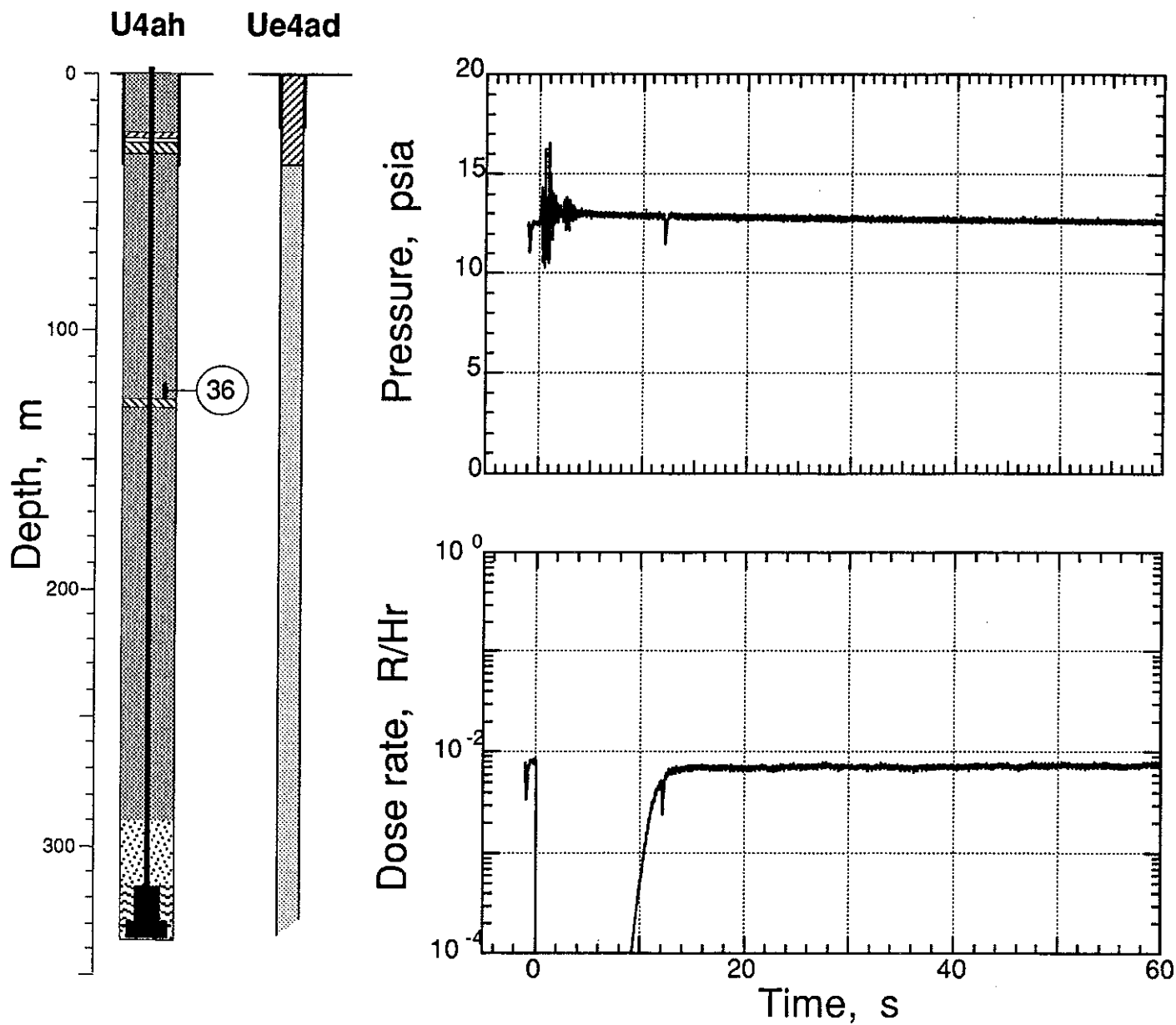


Figure 2.6 The first 60 s of pressure and radiation detected in the fines stemming of the emplacement hole above the rigid plug (Station 36 at a depth of 123 m). The radiation transducer was saturated by the EMP and began to recover about 12 s later.

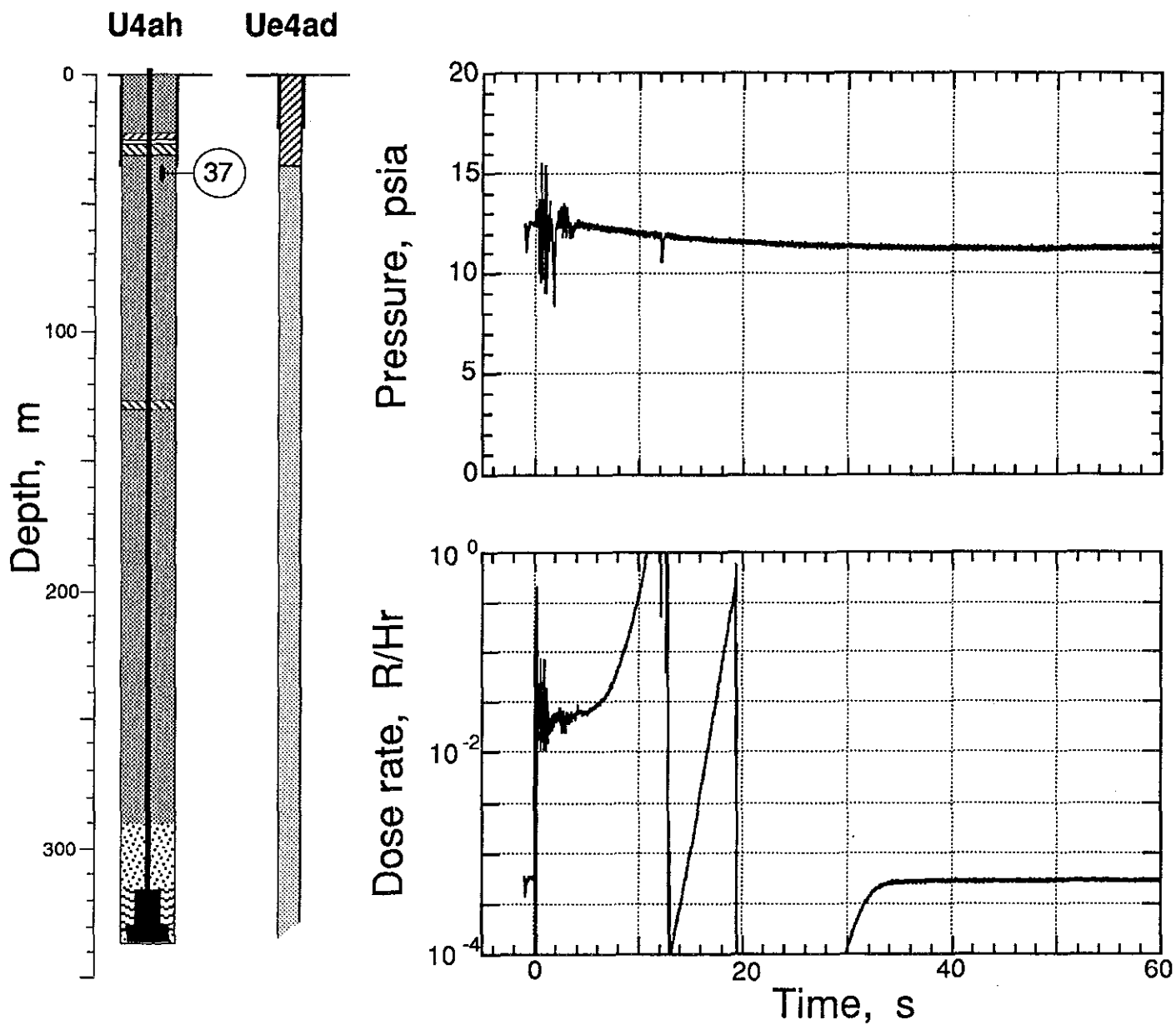


Figure 2.7 The first 60 s of pressure and radiation detected in the fines stemming of the emplacement hole below the top plug (Station 37 at a depth of 38 m). The radiation transducer was saturated by the EMP and began to recover about 30 s later.

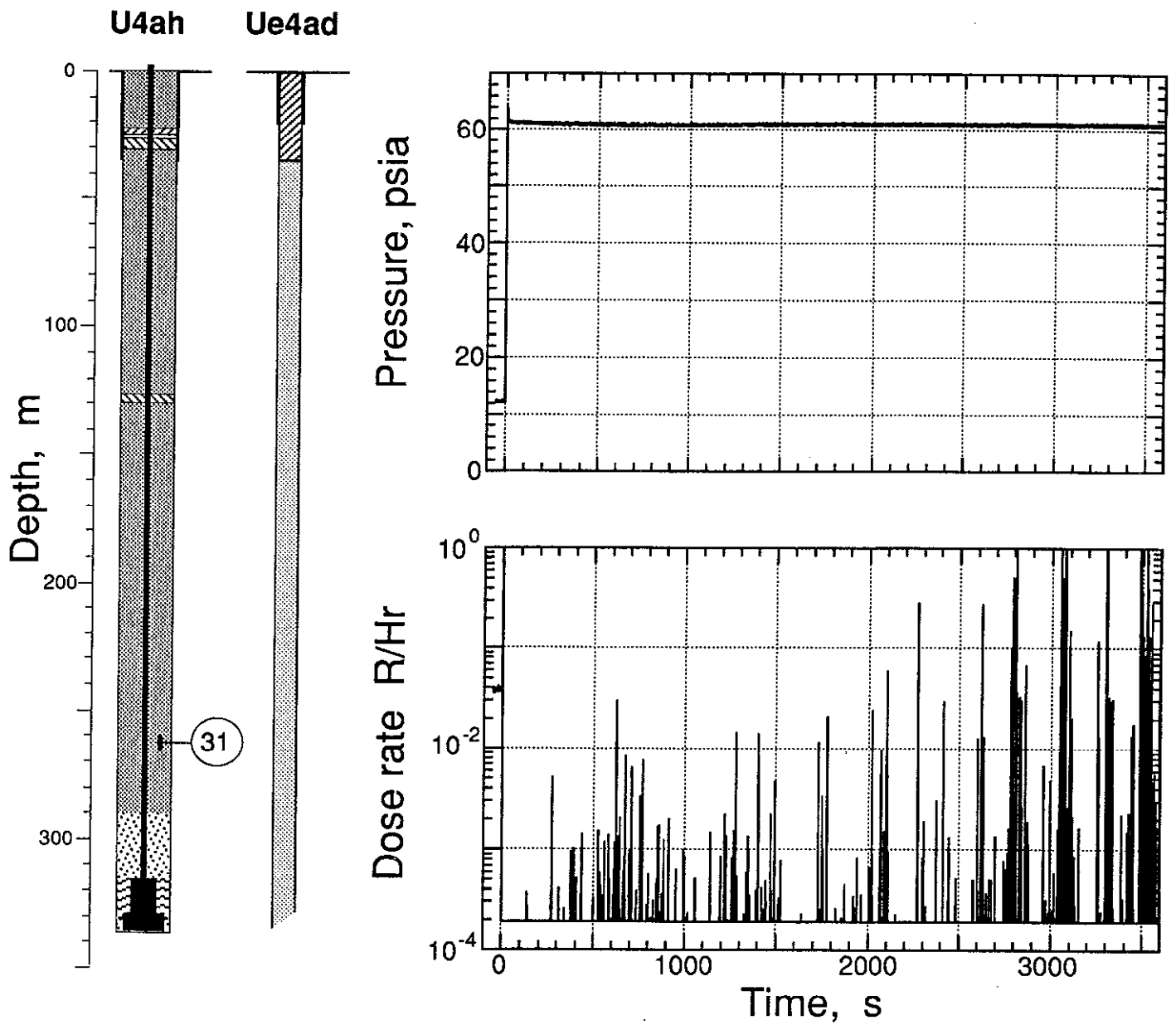


Figure 2.8 The first 3,600 s of pressure and radiation detected in the fines stemming of the emplacement hole (Station 31 at a depth of 262 m). The pressure record should not be accepted as it is above the system limits for the full time after denotation.

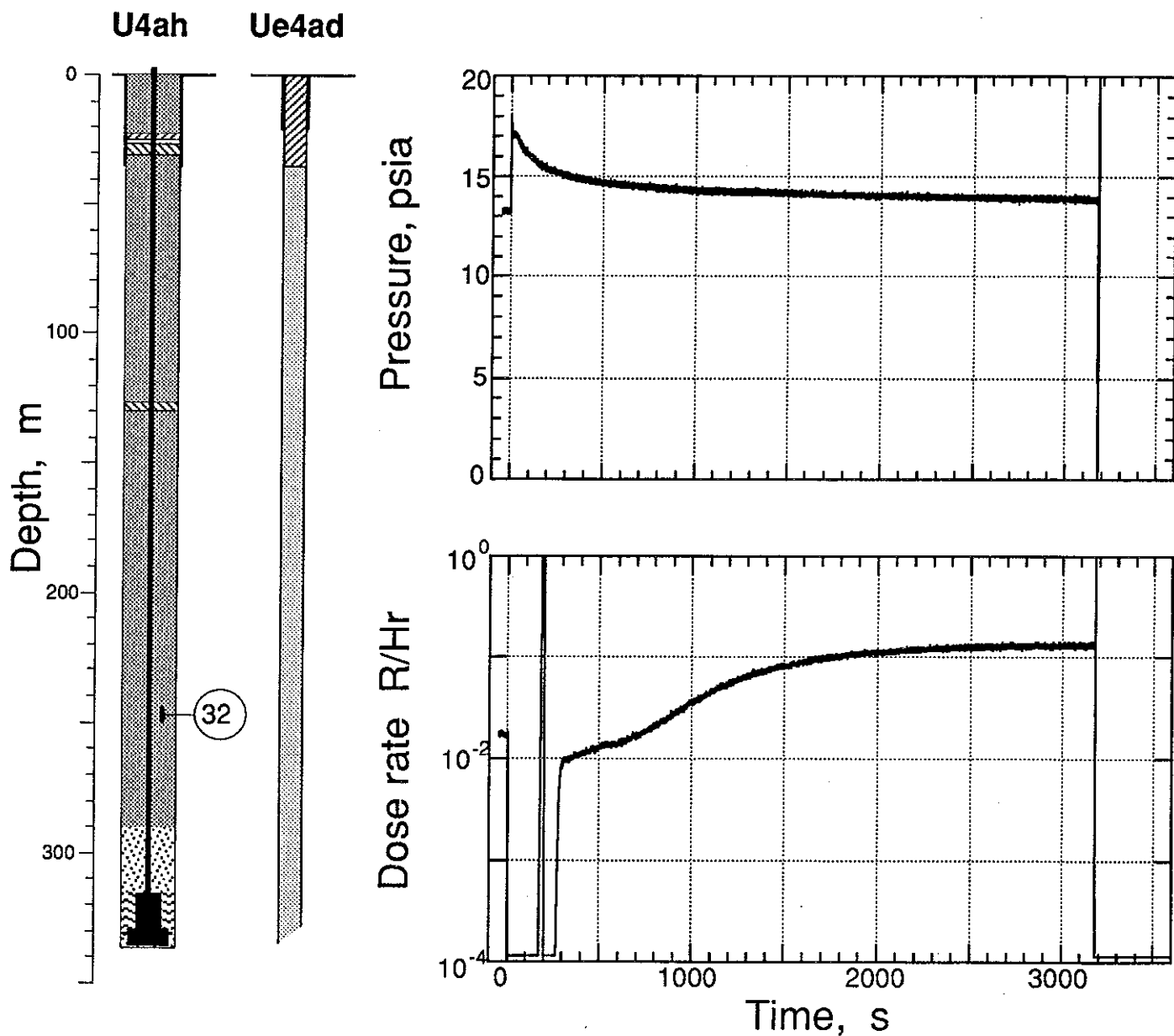


Figure 2.9 The first 3,600 s of pressure and radiation detected in the fines stemming of the emplacement hole (Station 32 at a depth of 247 m). The radiation transducer was saturated by the EMP and began to recover about 170 s later. A radiation arrival is seen at about 600 s.

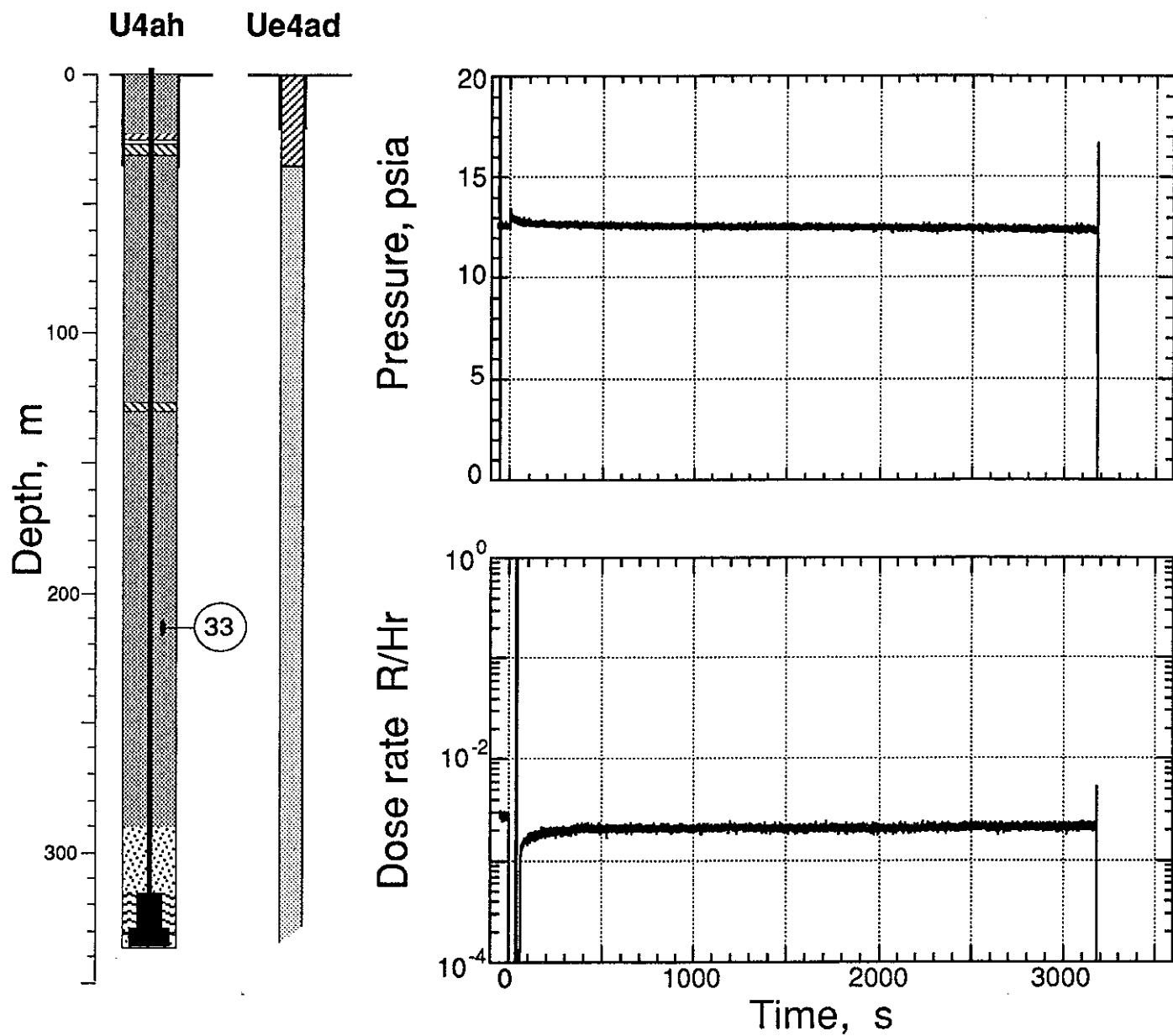


Figure 2.10 The first 3,600 s of pressure and radiation detected in the fines stemming of the emplacement hole (Station 33 at a depth of 213 m). The radiation transducer was saturated by the EMP and began to recover about 60 s later.

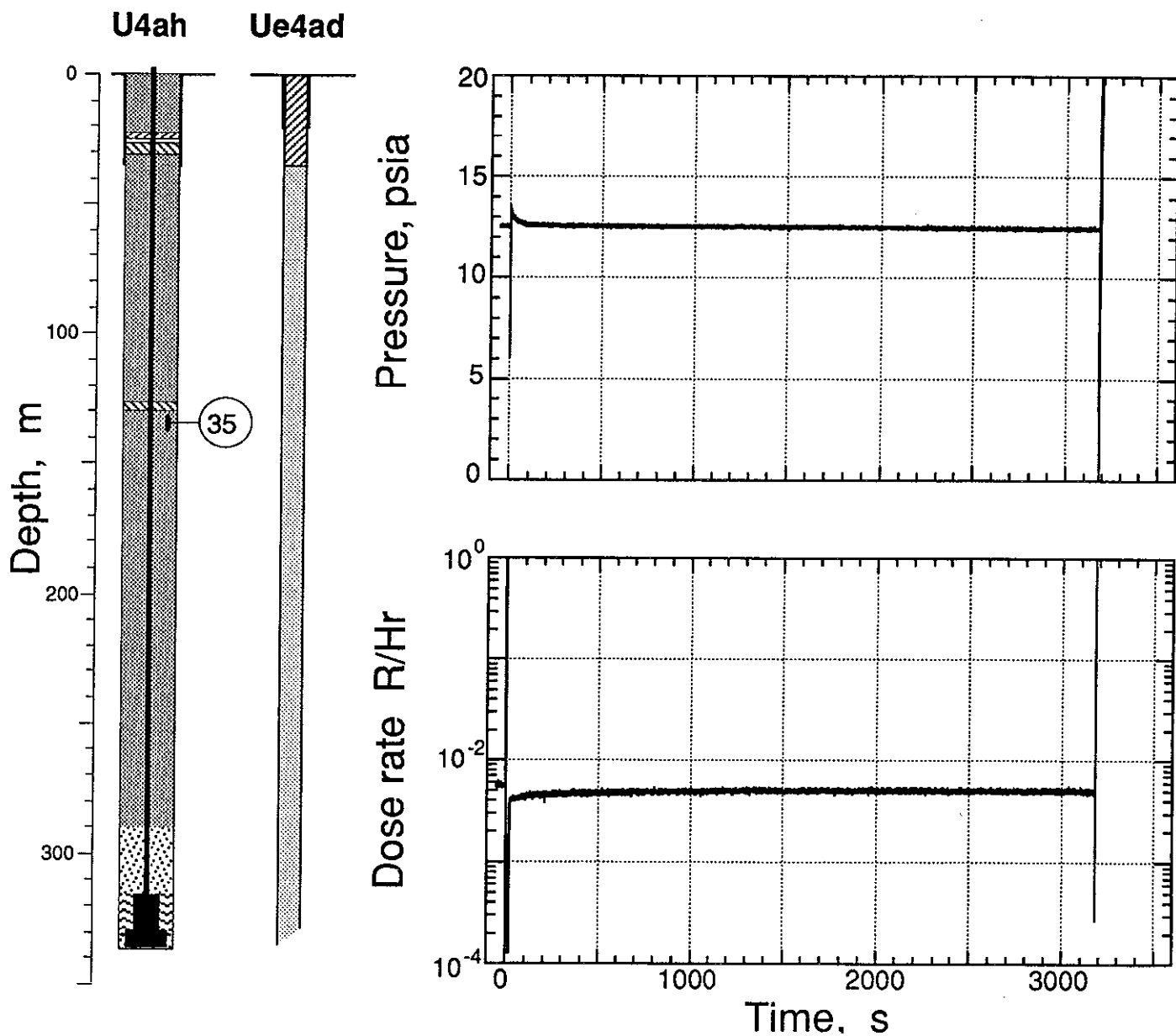


Figure 2.11 The first 3,600 s of pressure and radiation detected in the fines stemming of the emplacement hole below the rigid plug (Station 35 at a depth of 134 m). The radiation transducer was saturated by the EMP and began to recover about 20 s later.

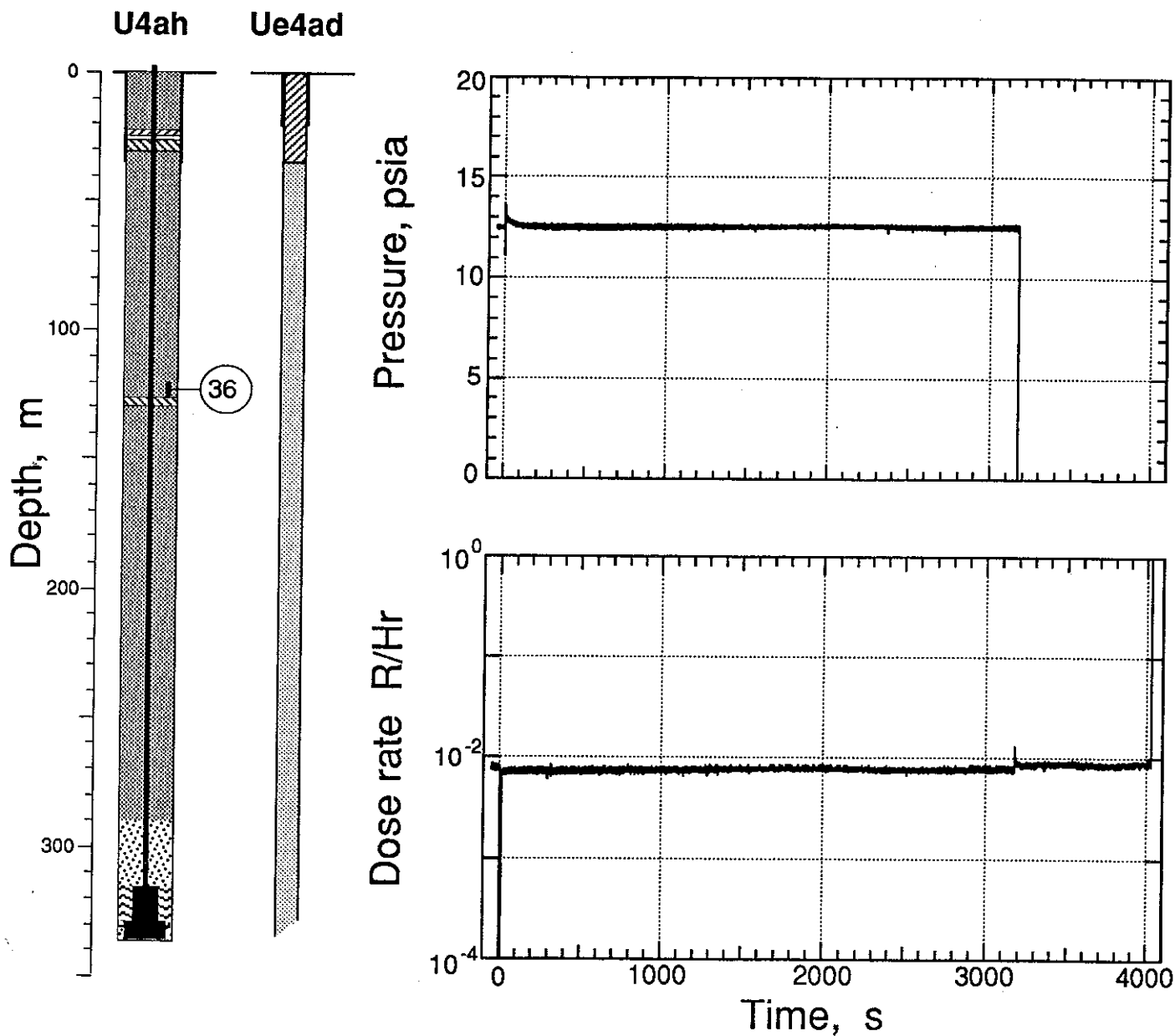


Figure 2.12 The first 4,100 s of pressure and radiation detected in the fines stemming of the emplacement hole above the rigid plug (Station 36 at a depth of 123 m). The radiation transducer was saturated by the EMP and began to recover about 12 s later and survived for about 900 s beyond the pressure transducer.

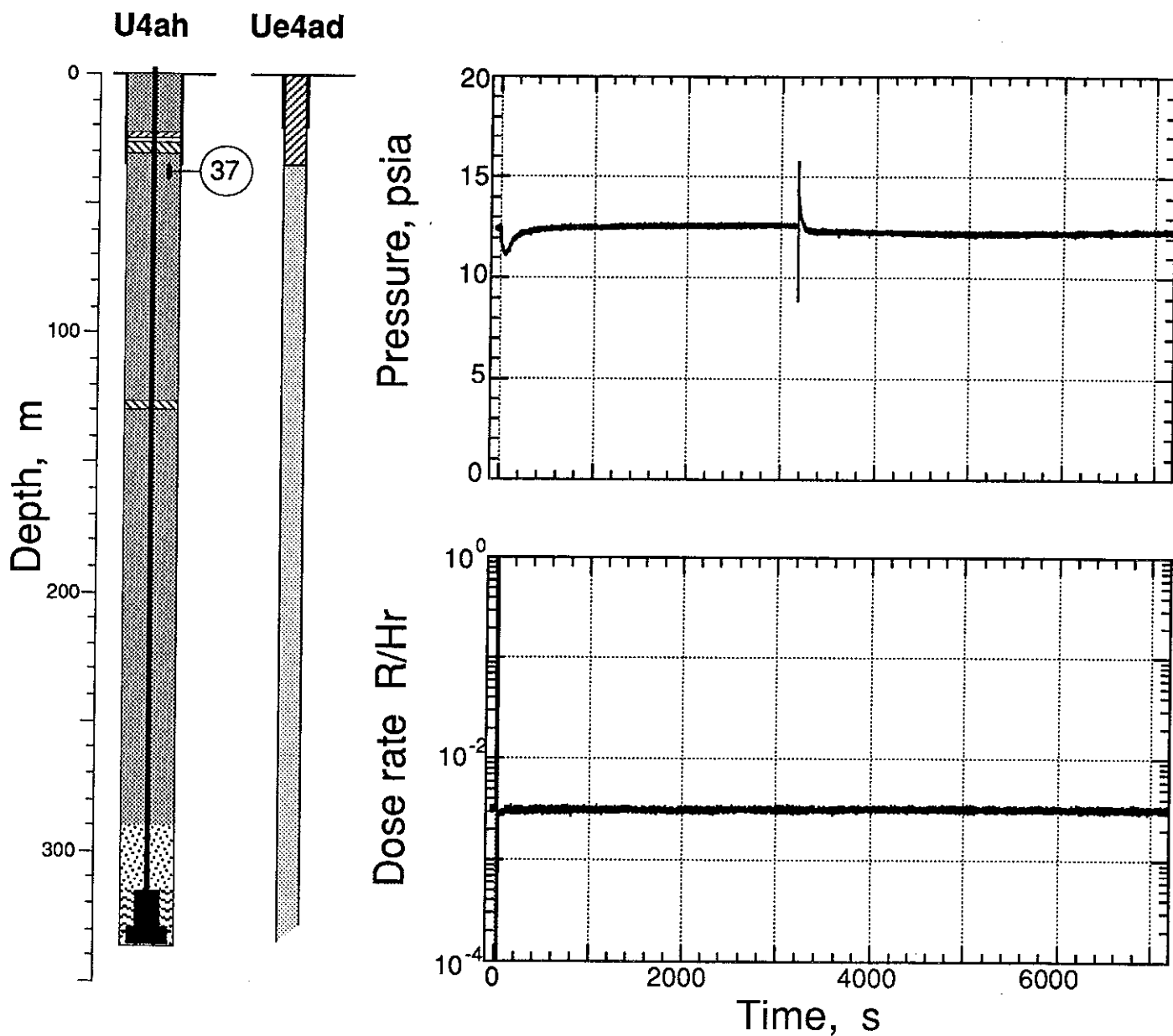


Figure 2.13 The pressure and radiation detected in the fines stemming of the emplacement hole below the top plug (Station 37 at a depth of 38 m). The radiation transducer was saturated by the EMP and began to recover about 32 s later. Both transducers survived the collapse.

2.2 Motion

The accelerometer at station 41 was disconnected pre-shot as it was causing interference in the rest of the motion transducer string. All other transducers at stations 40 and 41 and the accelerometer at station 44 were destroyed by the EMP and are not reported. Explosion-induced histories of the motion measured in the emplacement hole on the KARAB event are shown in figures 2.14–2.22. Characteristics of the associated motion and transducers are given in tables 2.1–2.3.

Agreement between the histories of the velocimeter and first integral of the acceleration is excellent at all stations, as are the displacement histories. Figure 2.23 and 2.24 depicts the range dependence of the peak acceleration while the range dependence of the first peak velocity is shown in figure 2.23. A least-squares fit to the data, represented by the straight lines shown in figures 2.23 and 2.24, gives the following results:

$$\text{Acceleration } A = 71,000 \times R^{-1.90[\pm 0.02]} \text{ g's}$$

$$\text{Velocity } U = 55 \times R^{-0.972[\pm 0.045]} \text{ m/s}$$

where R is slant range in meters.

During the time span of 0.3 to 0.4 s after detonation each of the accelerometers in the satellite hole at depth less than 160 m shows brief "noise" spikes that integrate away in the derived velocity. (See figures 2.17 - 2.21.) This phenomenon has been noted previously⁽⁴⁾ and was ascribed to relief of stress in the fiber glass pipe (locked in during grouting) on which the motion stations were hung. This happens when the motion wave reflects from the ground surface and the medium goes into dilatation.

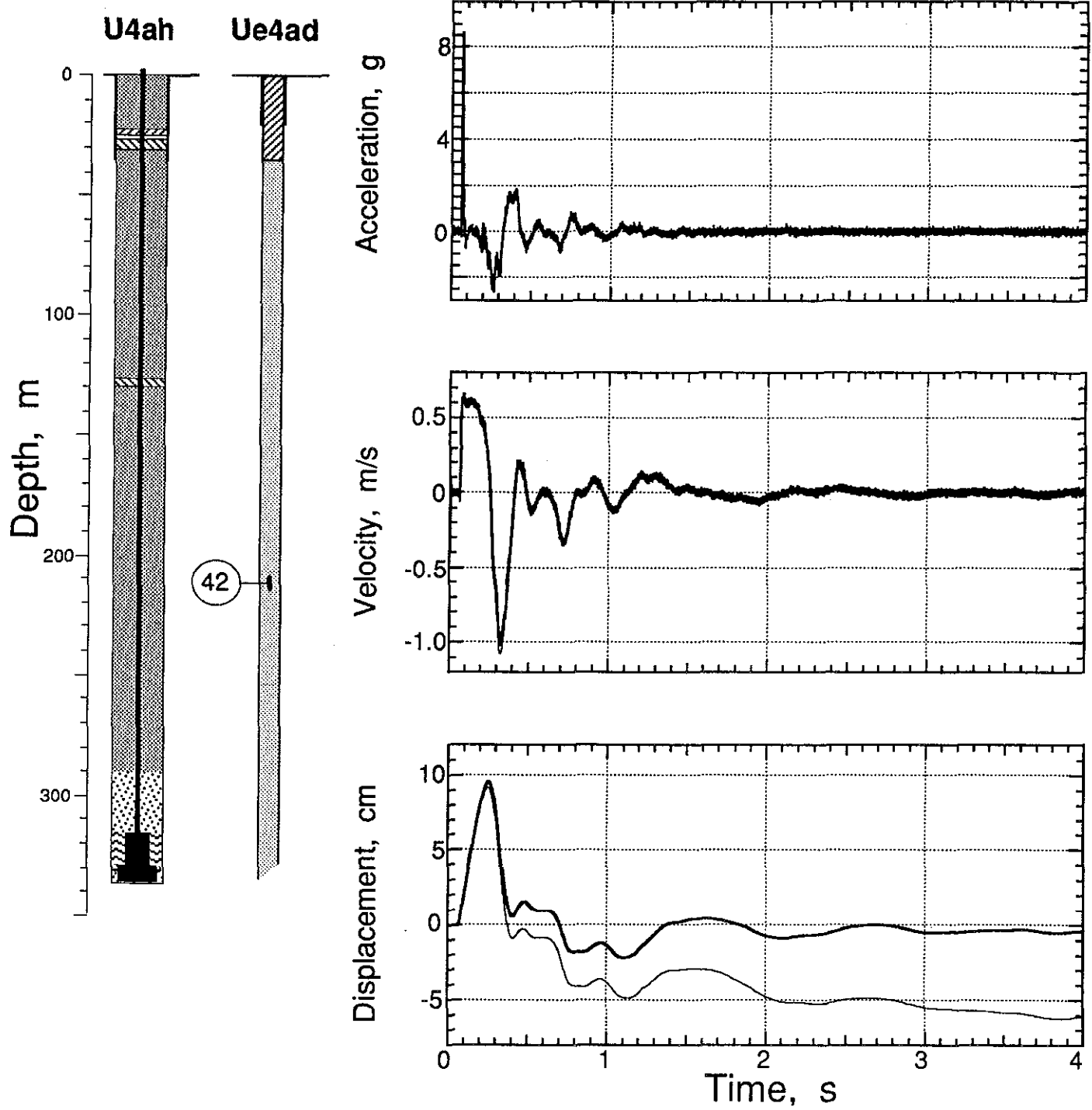


Figure 2.14 Explosion-induced motion in the satellite hole (station 42 at a depth of 211.5 m).

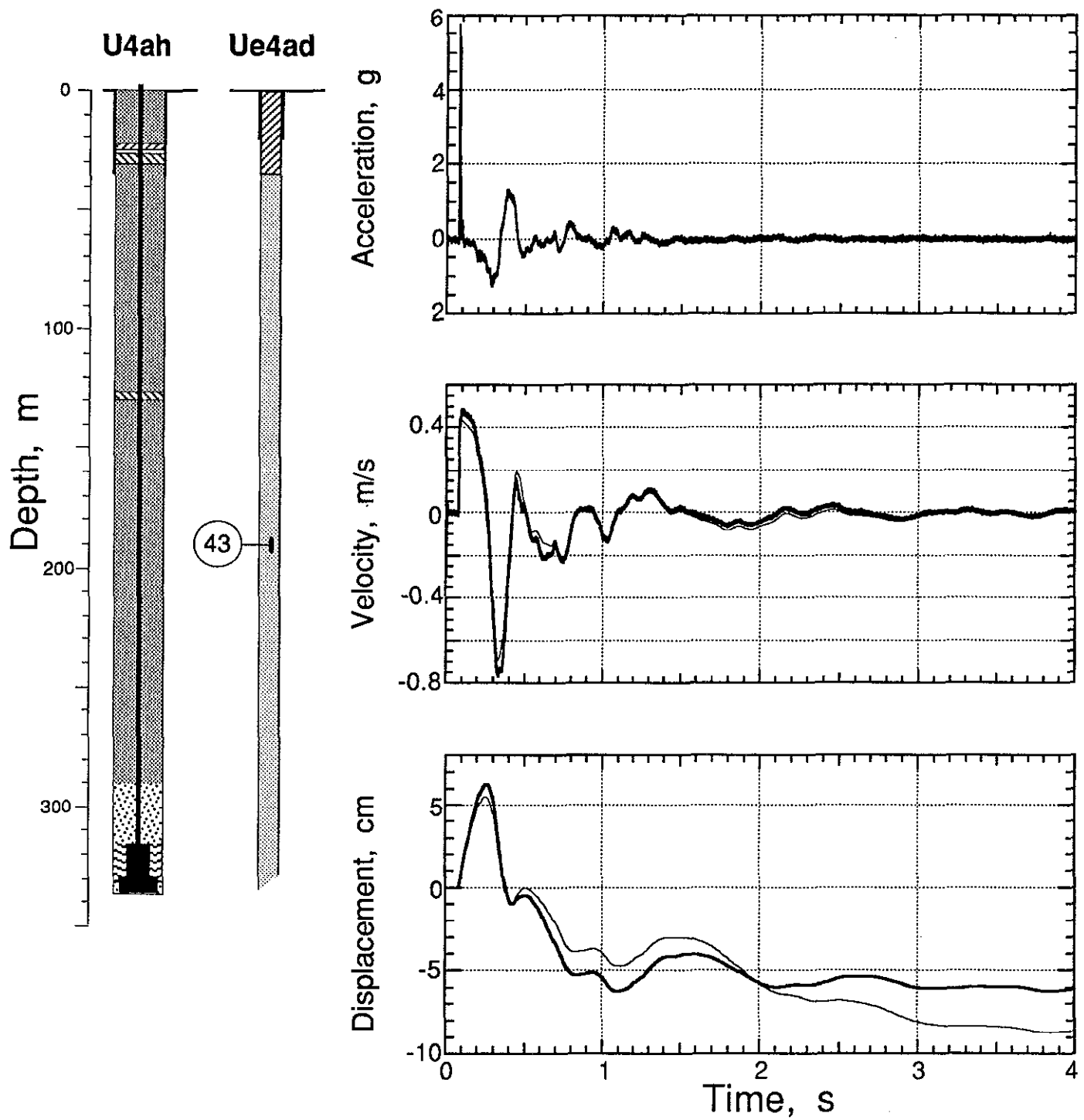


Figure 2.15 Explosion-induced motion in the satellite hole (station 43 at a depth of 190.2 m).

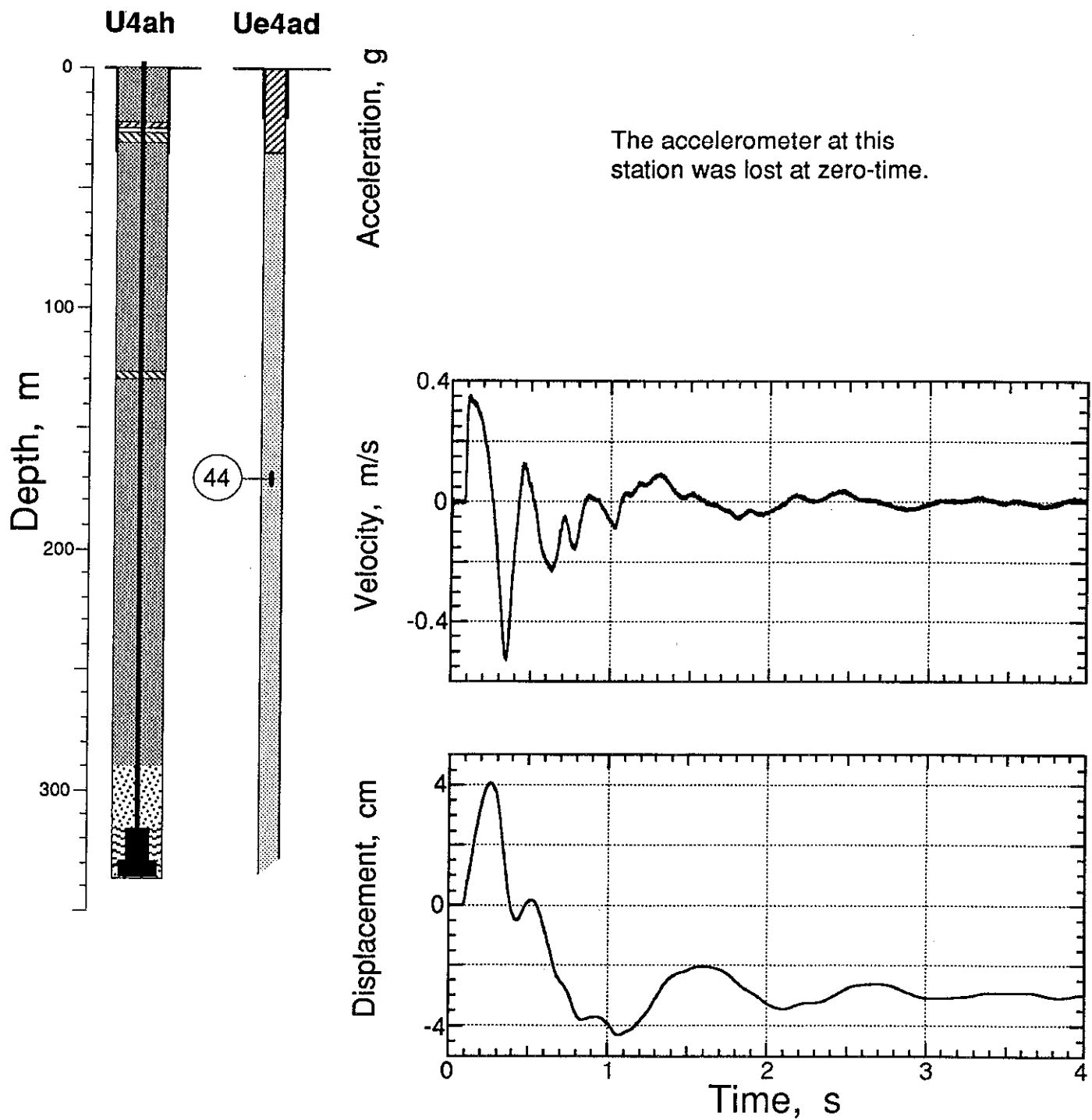


Figure 2.16 Explosion-induced motion in the satellite hole (station 44 at a depth of 170.3 m).

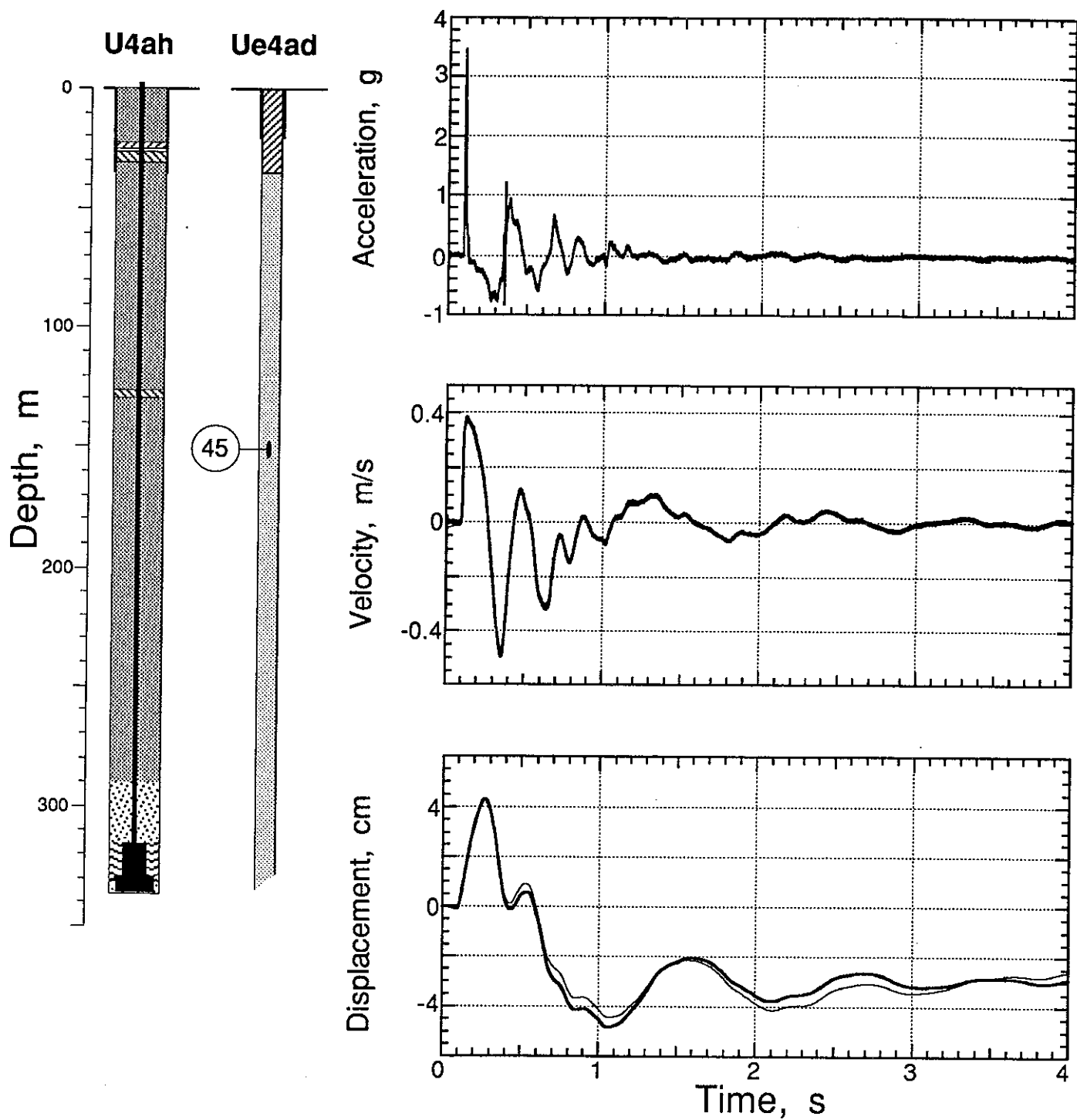


Figure 2.17 Explosion-induced motion in the satellite hole (station 45 at a depth of 150.4 m).

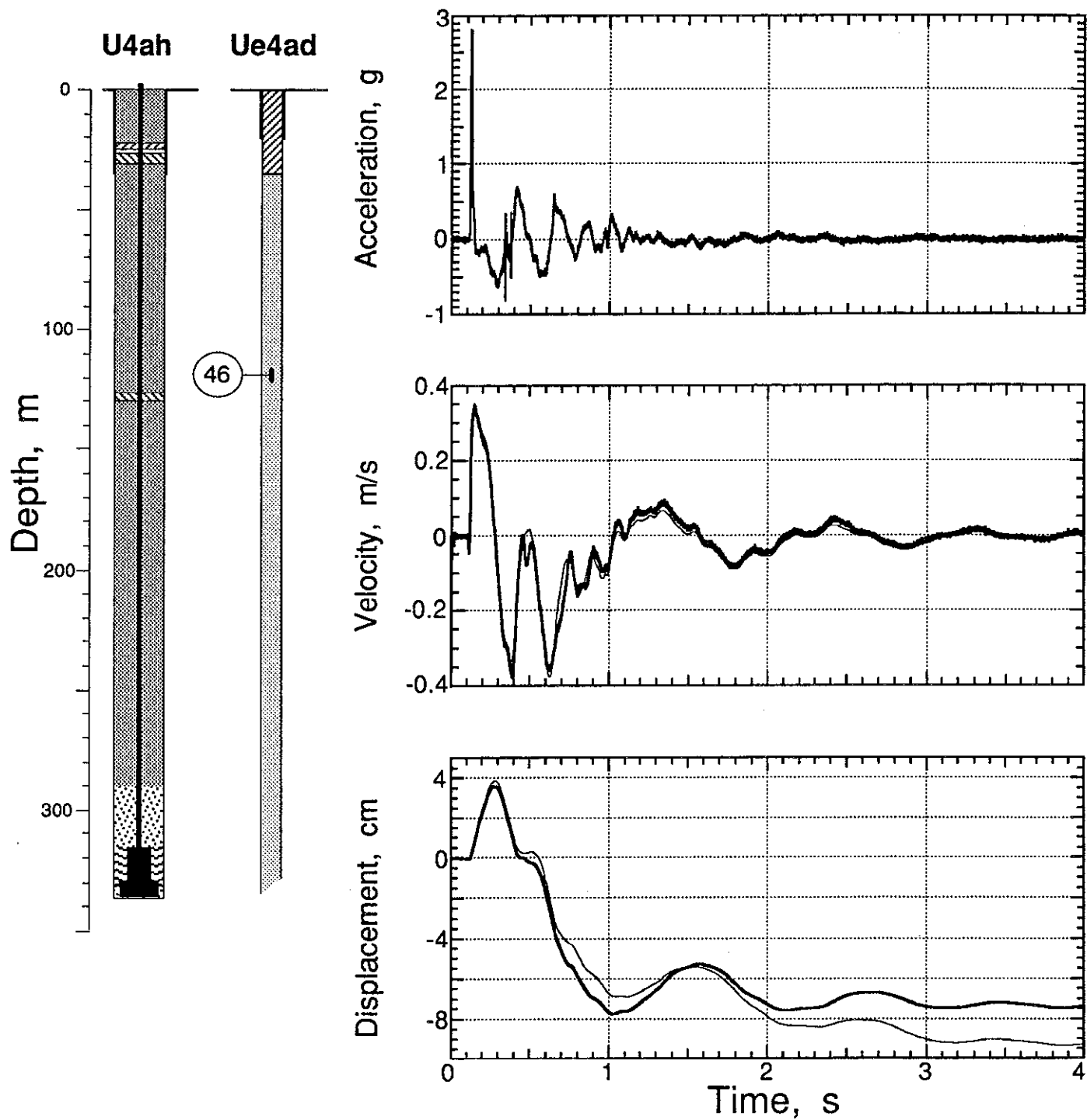


Figure 2.18 Explosion-induced motion in the satellite hole (station 46 at a depth of 119.1 m).

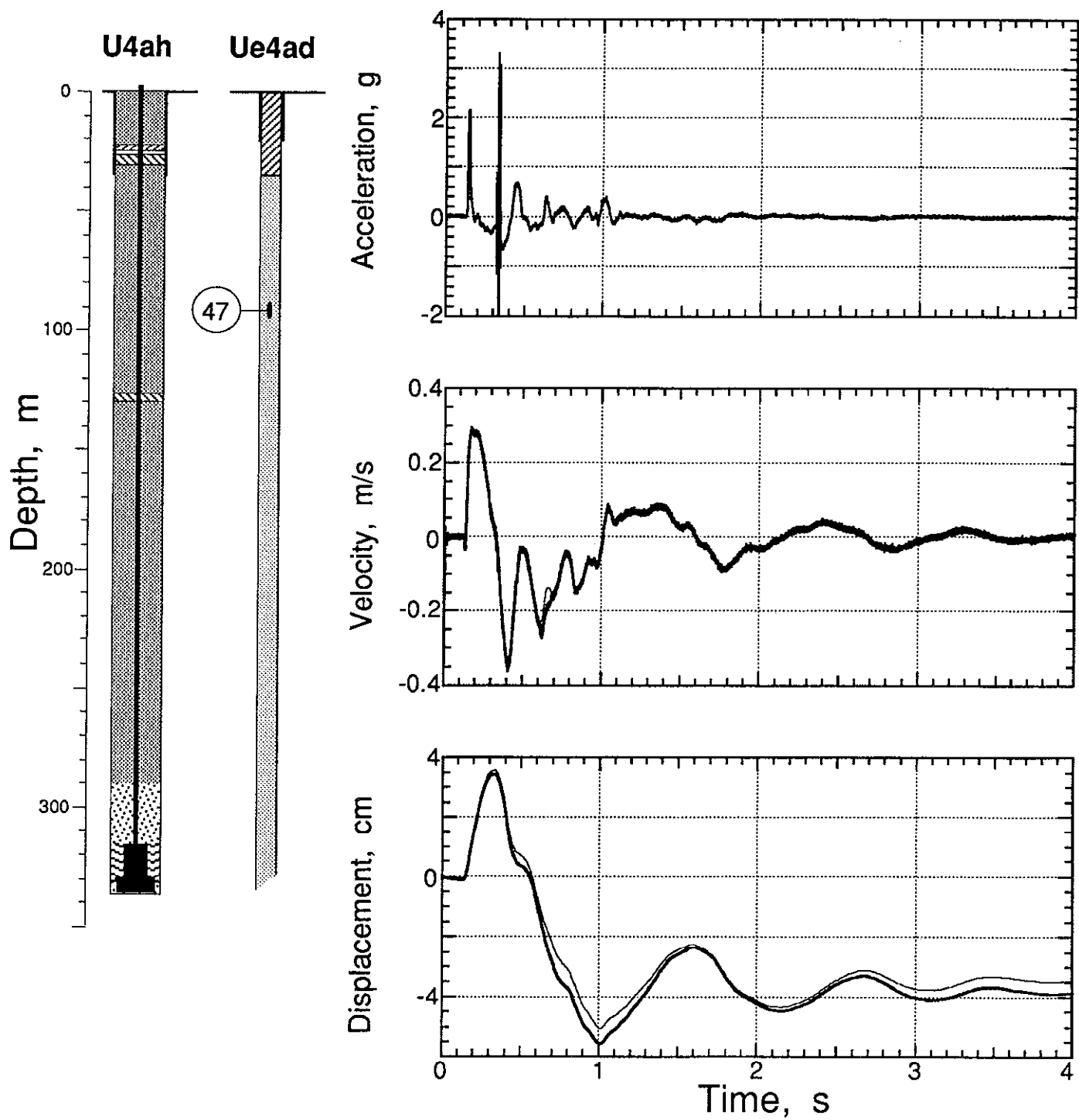


Figure 2.19 Explosion-induced motion in the satellite hole (station 47 at a depth of 90.8 m).

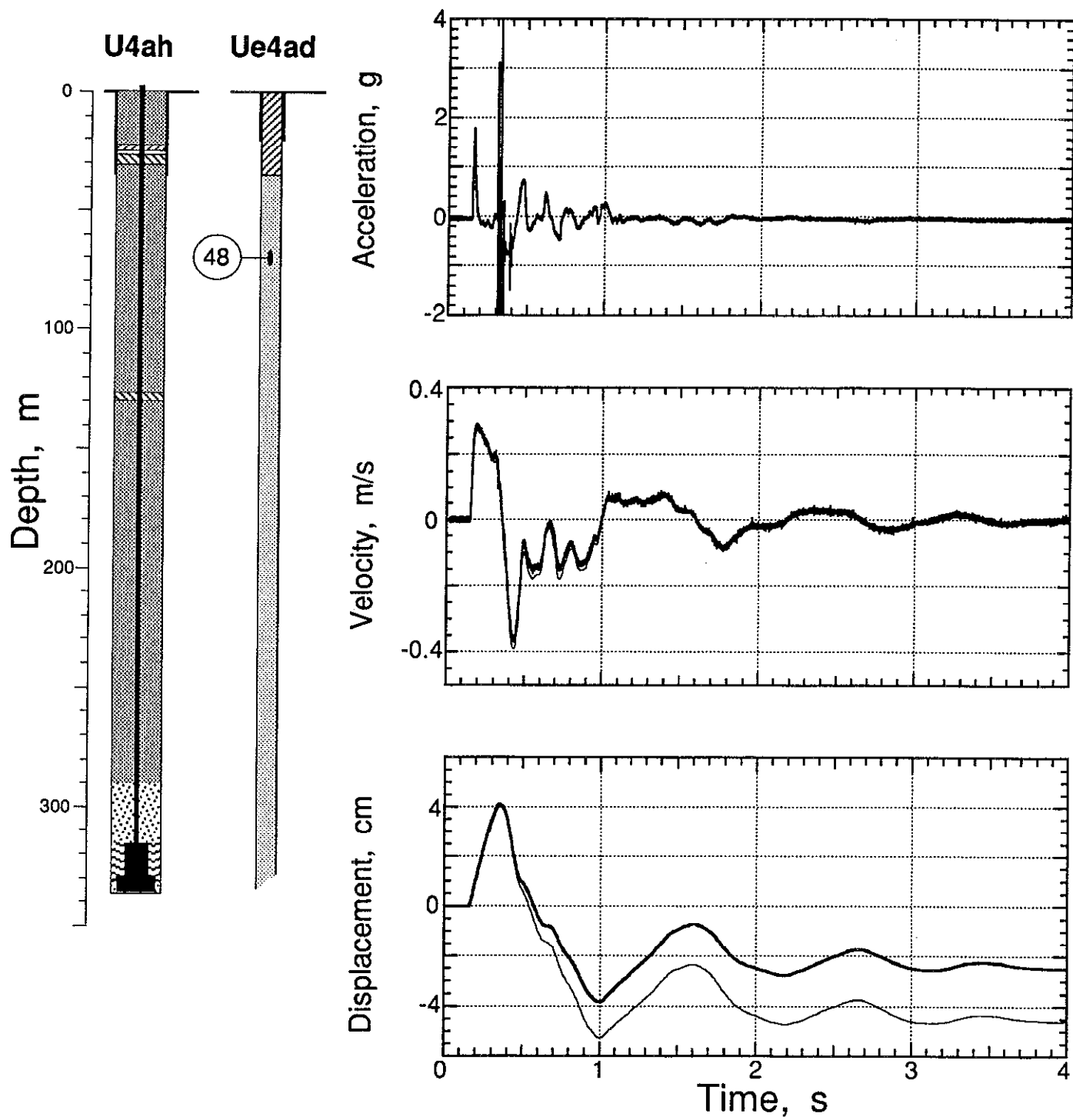


Figure 2.20 Explosion-induced motion in the satellite hole (station 48 at a depth of 70.0 m).

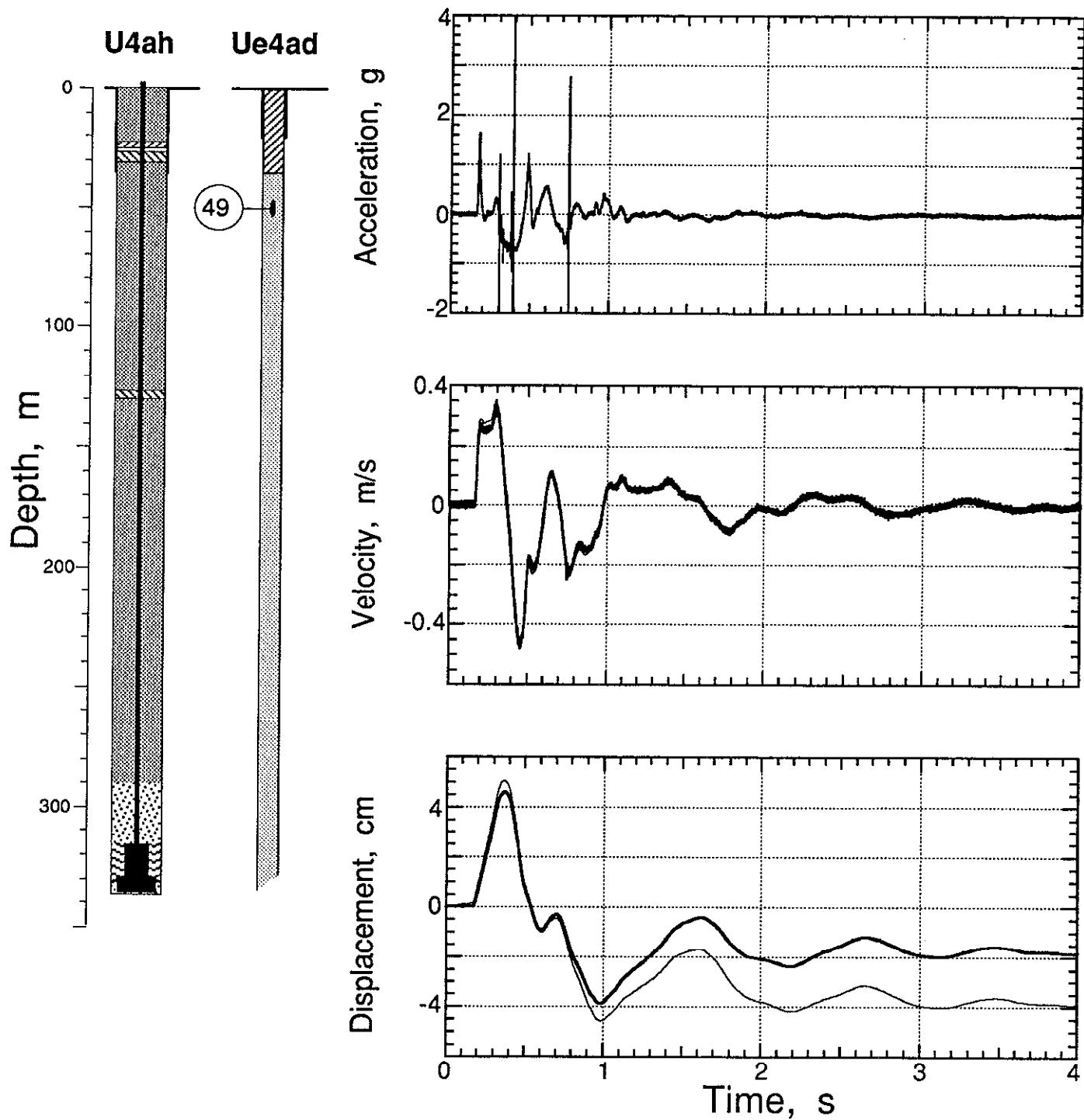


Figure 2.21 Explosion-induced motion in the satellite hole (station 49 at a depth of 50.2 m).

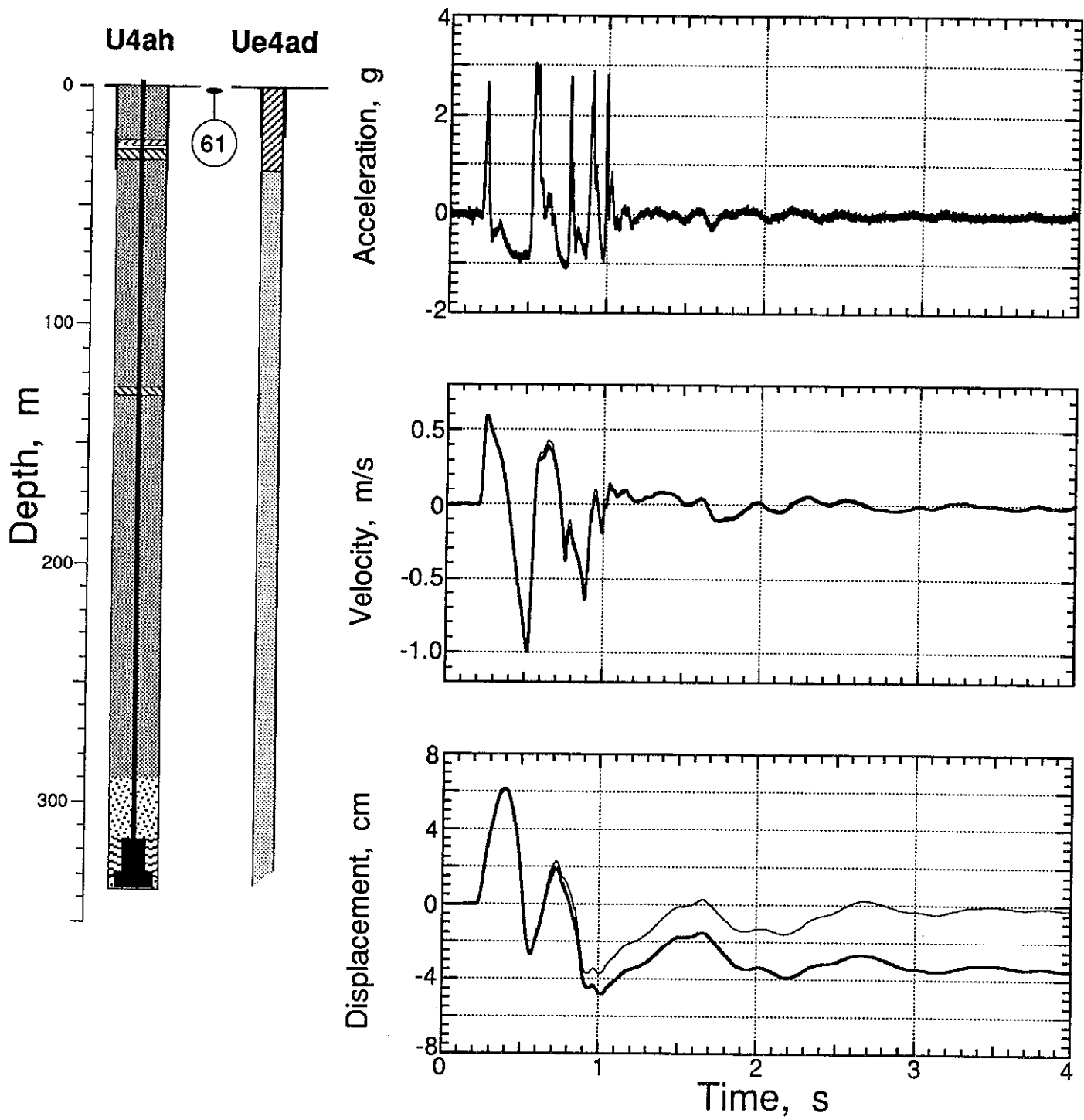


Figure 2.22 Explosion-induced motion of the ground surface (station 61 at horizontal range of 15.2 m and a depth of 0.91 m).

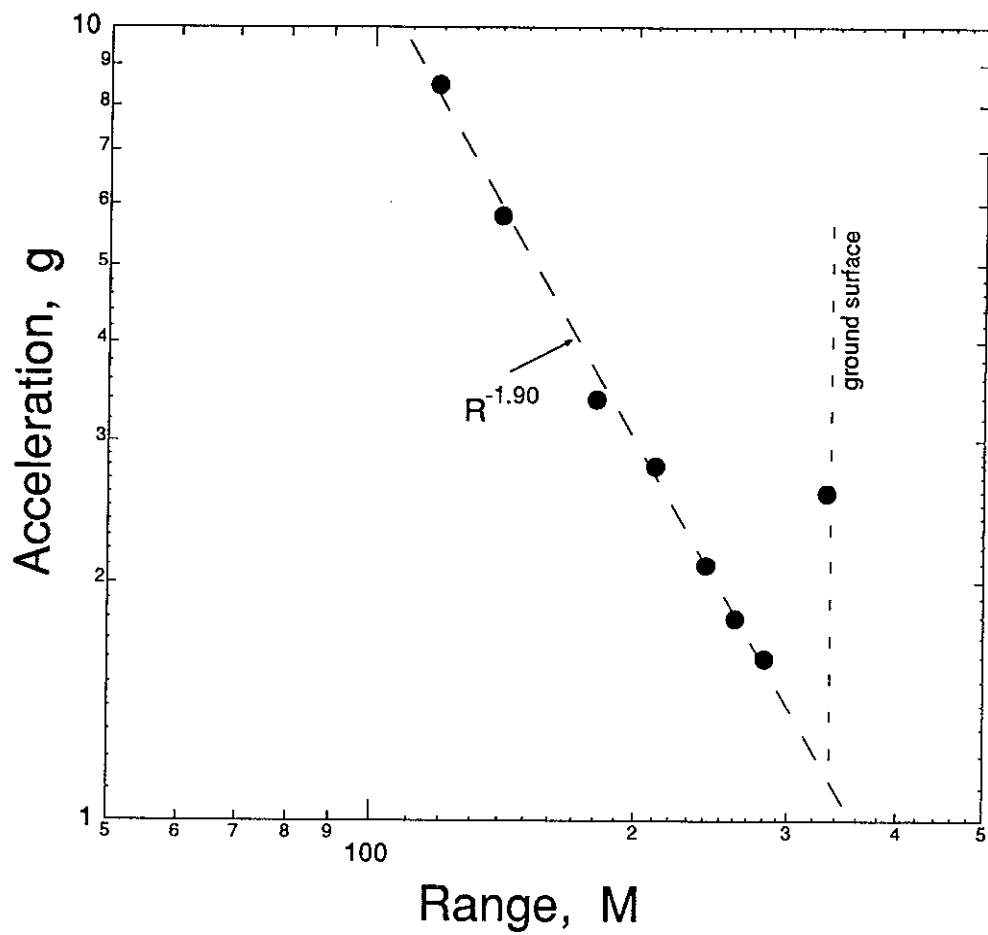


Figure 2.23 First peak vertical acceleration as a function of slant range from the explosive center. Based on seven data points, the exponent is -1.90 ± 0.02 .

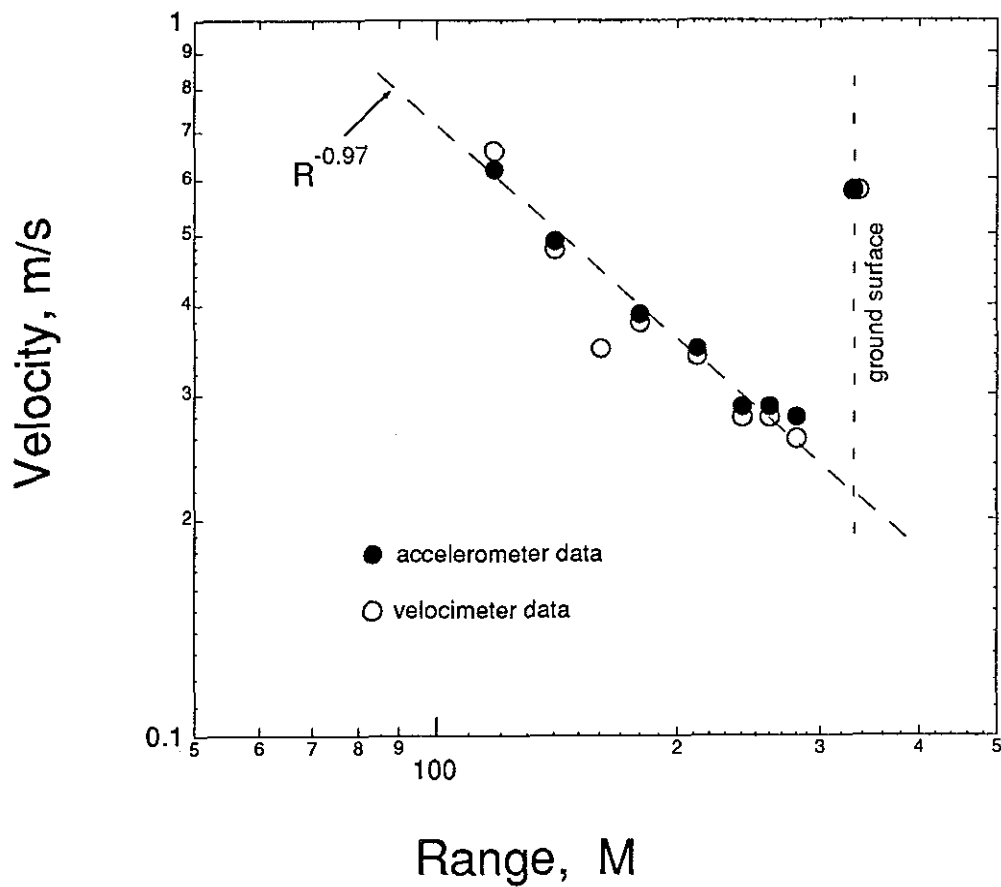


Figure 2.24 First peak vertical velocity as a function of slant range from the explosive center. Based on fourteen data points, the exponent is -0.972 ± 0.045 . The one datum at a range of 161 m was omitted as being too far beyond the standard deviation.

Table 2.1 Summary of Containment-Related Motion

Gauge	Slant Range (m)	Arrival Time (ms)	Acceleration Peak (g)	Velocity Peak (m/s)	Displacement Peak (cm)	Displacement Residual (cm)
40av(a)	67.5	-	-	-	-	-
40uv(a)	57.5	-	-	-	-	-
41av(b)	97.7	-	-	-	-	-
41uv(a)	97.7	-	-	-	-	-
42av	117.7	61	8.5	0.62	9.2	-1.3
42uv	117.7	61	-	0.66	9.6	-0.2
43av	139.9	74	5.8	0.49	6.3	-3.7
43uv	139.9	75	-	0.48	5.5	-4.5
44av(a)	160.6	-	-	-	-	-
44uv	160.6	85	-	0.35	4.0	-3.0
45av	180.1	95	3.4	0.39	4.3	-3.4
45uv	180.1	97	-	0.38	4.3	-5.4
46av	210.3	114	2.8	0.35	3.8	-4.8
46uv	210.3	115	-	0.34	3.9	-6.7
47av	240.5	134	2.1	0.29	3.6	-4.5
47uv	240.5	134	-	0.28	3.4	-4.8
48av	260.6	147	1.8	0.29	4.2	-1.5
48uv	260.6	148	-	0.28	4.1	-2.3
49av	280.7	162	1.6	0.28	5.0	-3.5
49uv	280.7	163	-	0.26	4.9	-1.4
61av	330.0	206	2.6	0.58	6.2	-2.0
61uv	330.0	208	-	0.58	6.2	-3.5

(a) Destroyed by ZIP.

(b) Disconnected pre-shot.

Table 2.2 Containment-Related Accelerometer Characteristics

Gauge	Natural Frequency (Hz)	Damping Ratio	System Range (g's)
40av	1800	0.65	800
41av	800	0.65	120
42av	680	0.65	100
43av	350	0.70	40
44av	260	0.70	20
45av	300	0.70	20
46av	300	0.65	20
47av	290	0.65	20
48av	300	0.70	20
49av	240	0.75	20
61av	315	0.65	30

Table 2.3 Containment-Related Velocimeter Characteristics

Gauge	Natural Frequency (Hz)	Time to 0.5 Amplitude (s)	Calibration Temperature (°F)	Operate Temperature (°F)	System Range (m/s)
40uv(a)	3.70	22.2	73.5	72.8	50
41uv	3.18	8.4	74.5	70.8(b)	16
42uv	3.54	6.9	74.0	69.3	10
43uv	3.57	8.5	74.2	68.6	4
44uv	3.50	8.17	74.4	68.0	4
45uv	2.81	19.2	74.0	67.1	2
46uv	2.91	16.8	73.9	65.8	2
47uv	2.99	30.5	74.3	64.7	3
48uv	3.39	10.6	74.2	64.5	4
49uv	3.47	14.7	75.0	64.1	4
61uv	3.64	8.20	72.9	48.2	4

(a) Aluminum pendulum.

(b) Measured value not available: Interpolated from surrounding points.

3 Collapse phenomena

All stations in the emplacement hole registered the effects of a surface collapse occurring about 3175 s after detonation.

3.1 Pressure and radiation

Pressure and radiation wave forms obtained from the five stations in the stemming that survived until collapse are shown for a time period spanning the collapse episode (3160 s to 3190 s) are shown in figures 3.1 - 3.5. Pressure histories from these five stations are also shown in the composite plot figure 3.15. Signals were lost from all stations at elevations deeper than the one just below the top plug (station 37), presumably due to cable breakage.

All stations indicate collapse by a slow pressure drop toward zero followed by an abrupt signal loss or re-compaction to higher than ambient suggesting the termination of fall. Station 35 (figure 3.3) is anomalous possibly since the sample rate was insufficient to fully describe the wave form.

The surviving station 37 (figures 3.5 and 2.12) shows the characteristic pressure wave form of stemming fall and recompaction due to collapse. The slight change in radiation level indicated in figure 2.12 around collapse is attributed to motion of the source chip relative to the detector.

No radiation arrivals were observed above ground at any time after the KARAB event and the data are consistent with satisfactory containment.

3.2 Motion

The collapse-induced motion associated with the emplacement hole detected on KARAB is shown in figures 3.6-3.14. The system limits were exceeded on all the velocity channels for stations 21 and 61 and no associated accelerations were processed. The displacement histories of all the stations are shown in the composite plot of figure 3.15, describing the progression of the cavity collapse in both the emplacement and satellite holes.

No CLIPER data are available for inclusion in figure 3.15.

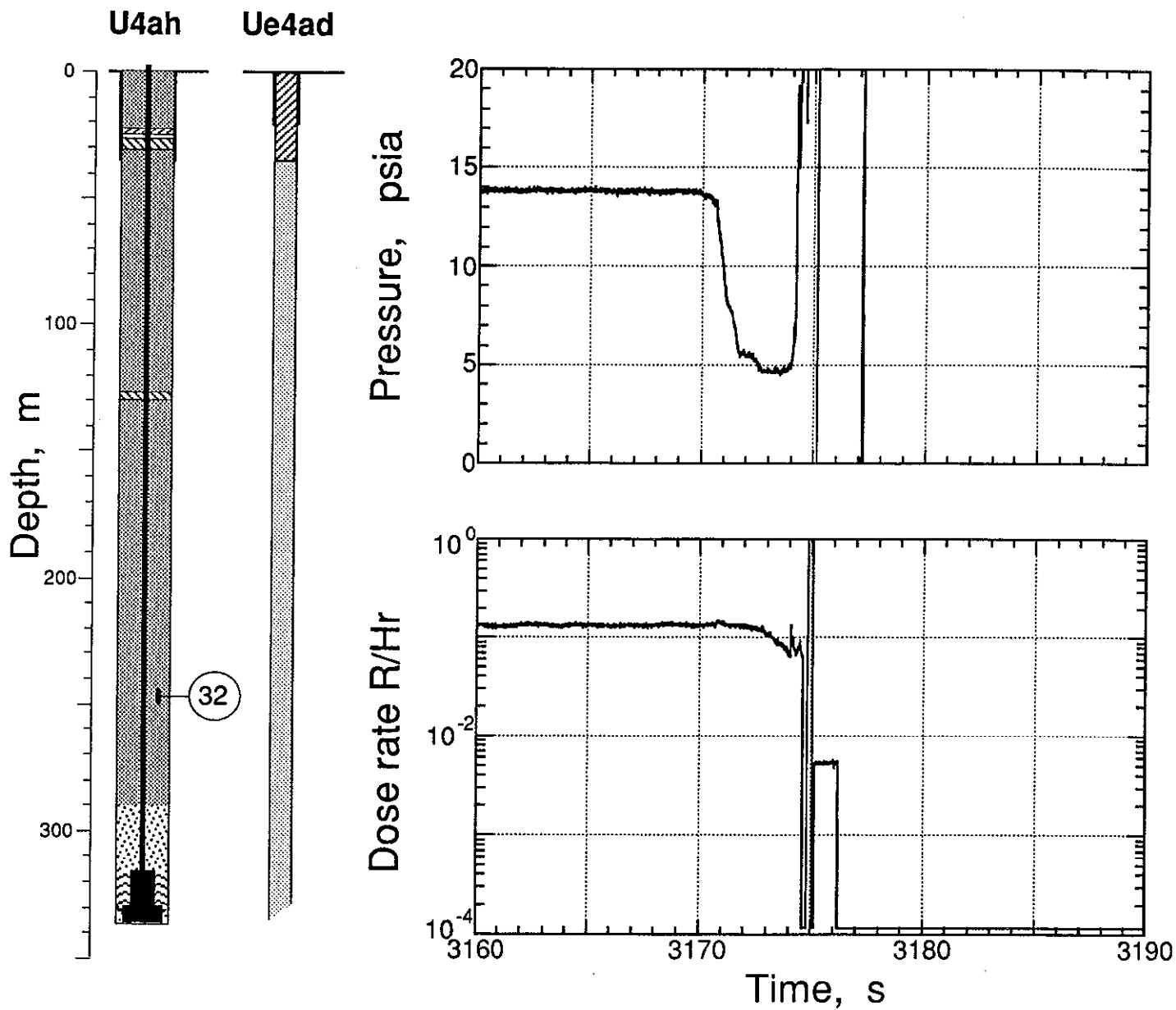


Figure 3.1 Collapse epoch pressure and radiation measured in the stemming of the emplacement hole (station 32 at a depth of 247 m).

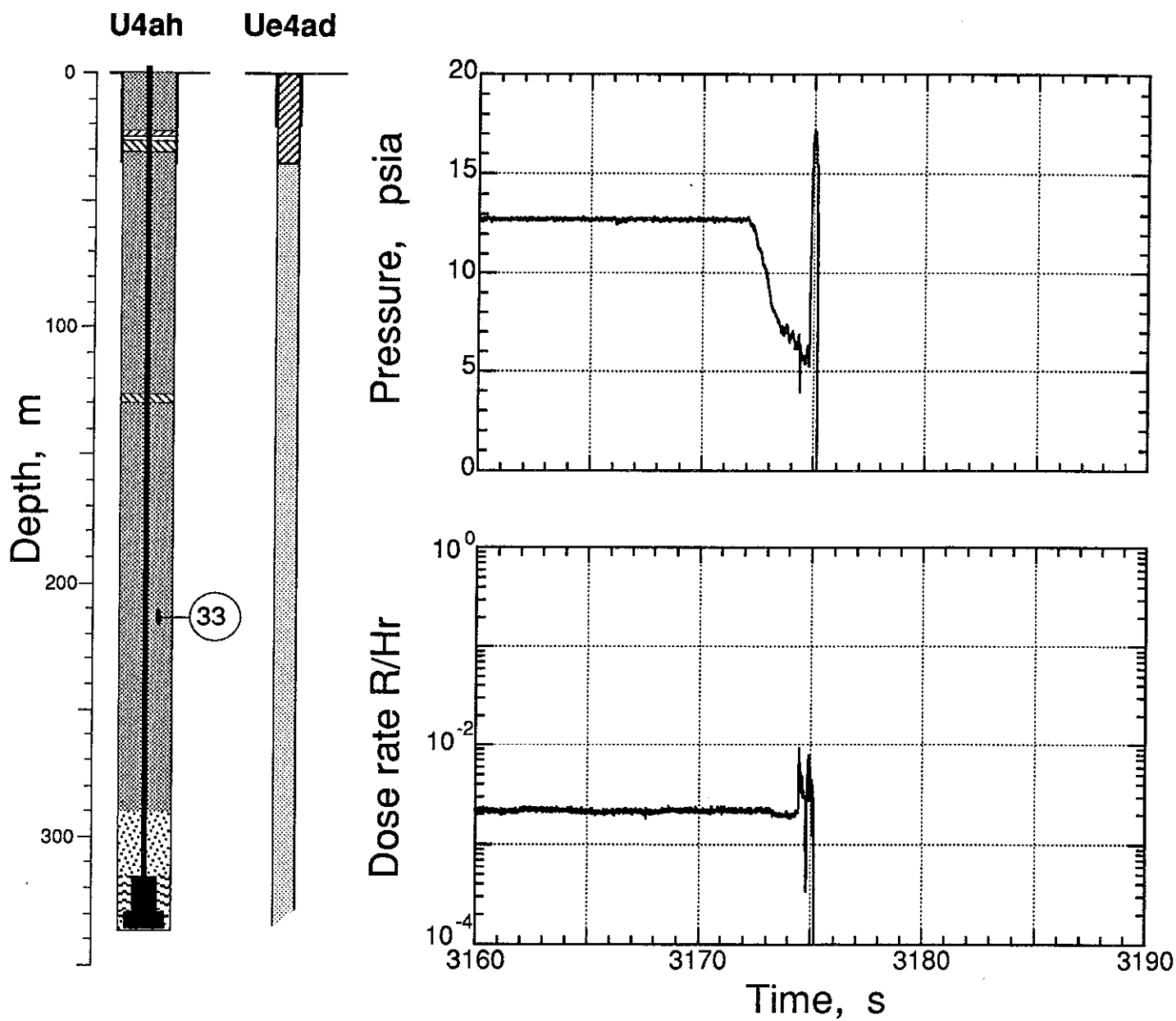


Figure 3.2 Collapse epoch pressure and radiation measured in the stemming of the emplacement hole (station 33 at a depth of 213 m).

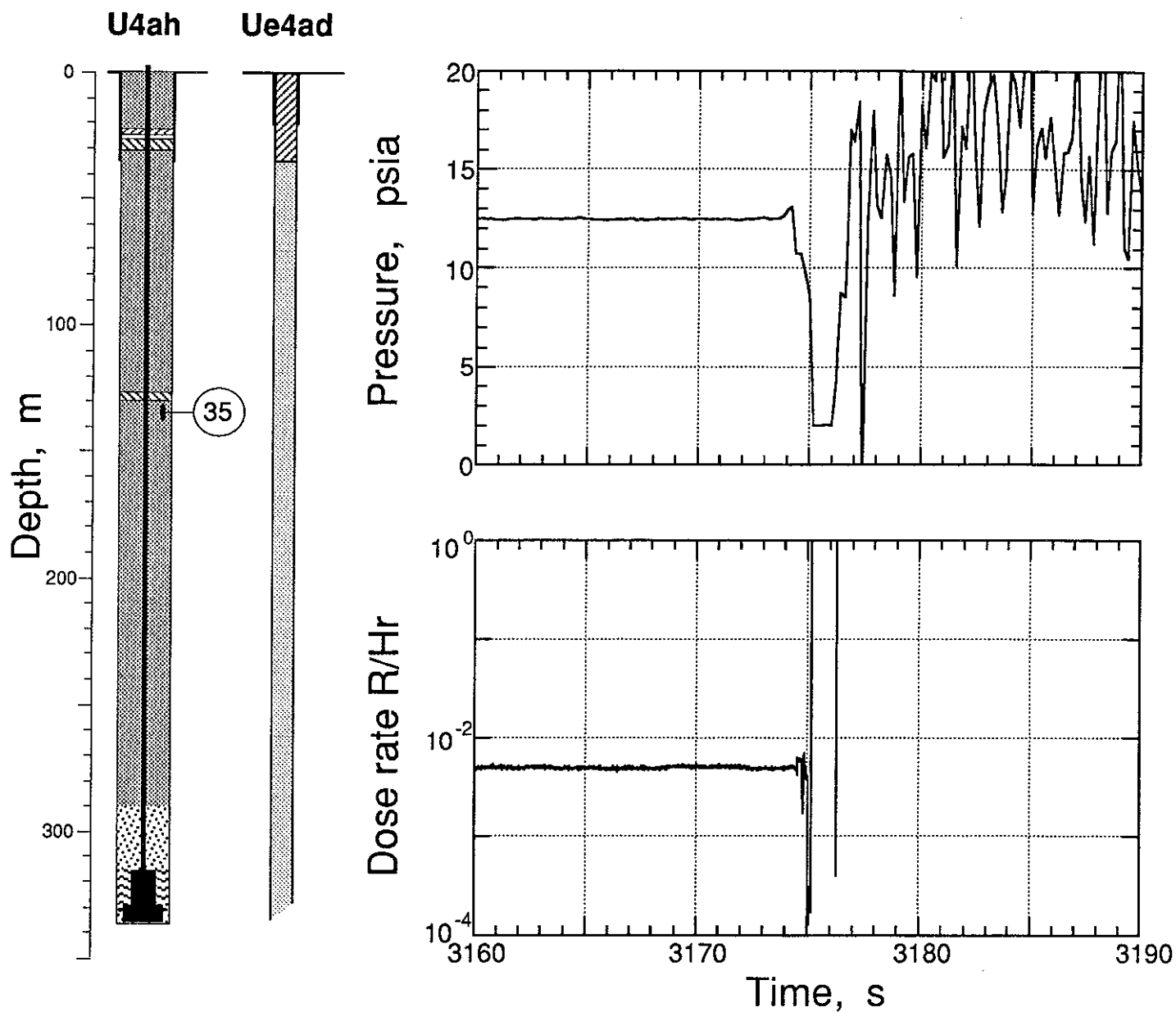


Figure 3.3 Collapse epoch pressure and radiation measured below the stemming platform (station 35 at a depth of 134 m).

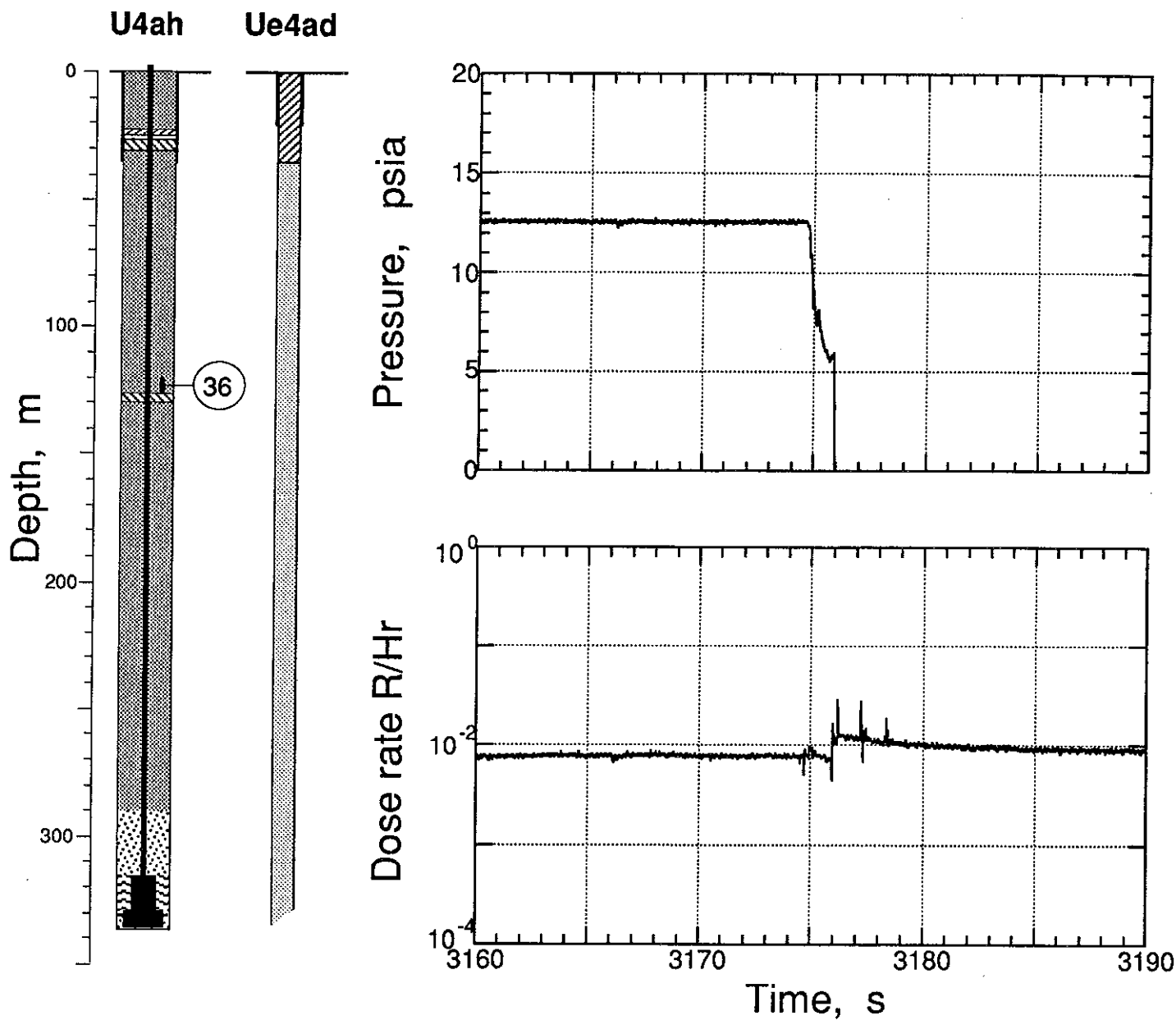


Figure 3.4 Collapse epoch pressure and radiation measured above the stemming platform (station 36 at a depth of 123 m).

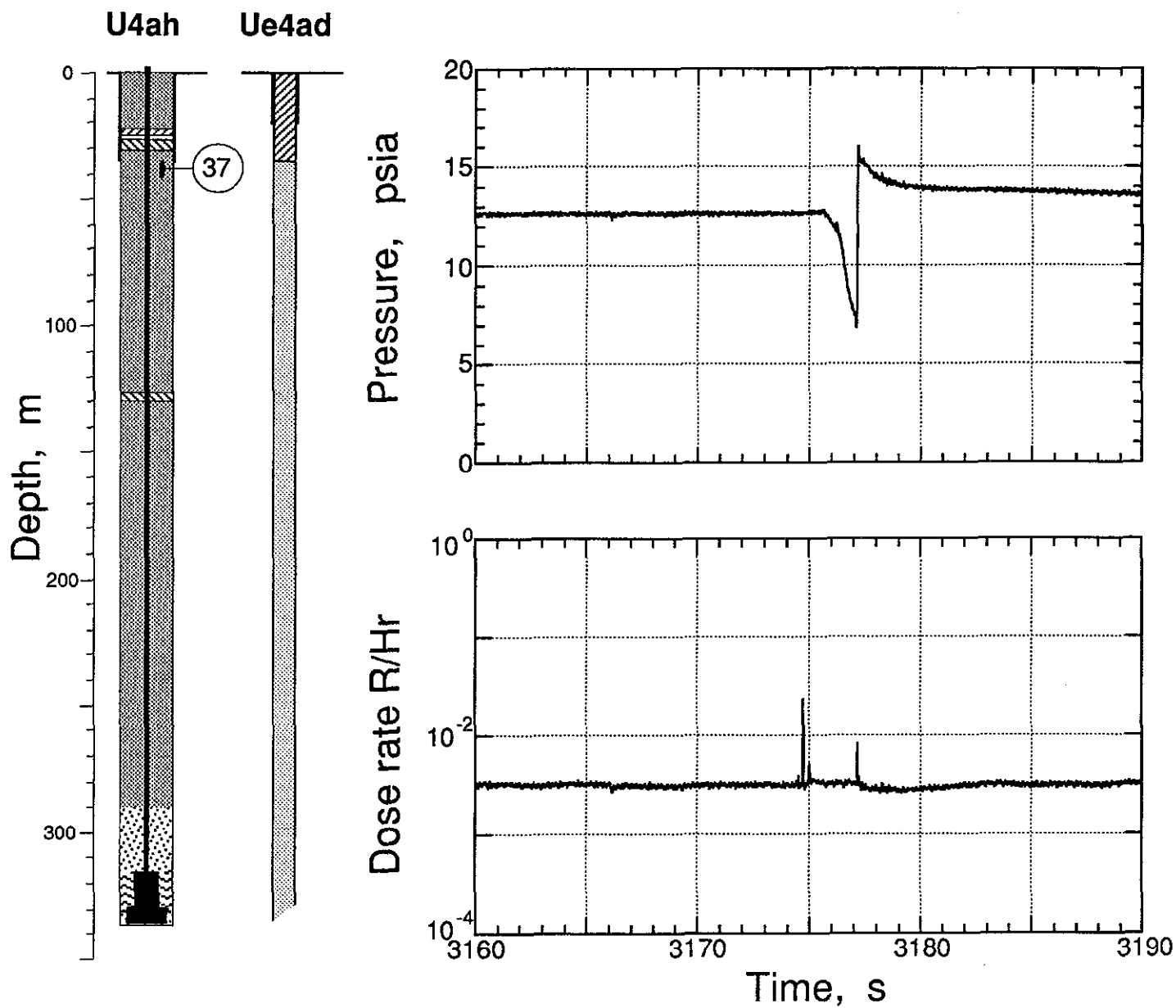


Figure 3.5 Collapse epoch pressure and radiation measured in the stemming of the emplacement hole (station 37 at a depth of 38 m).

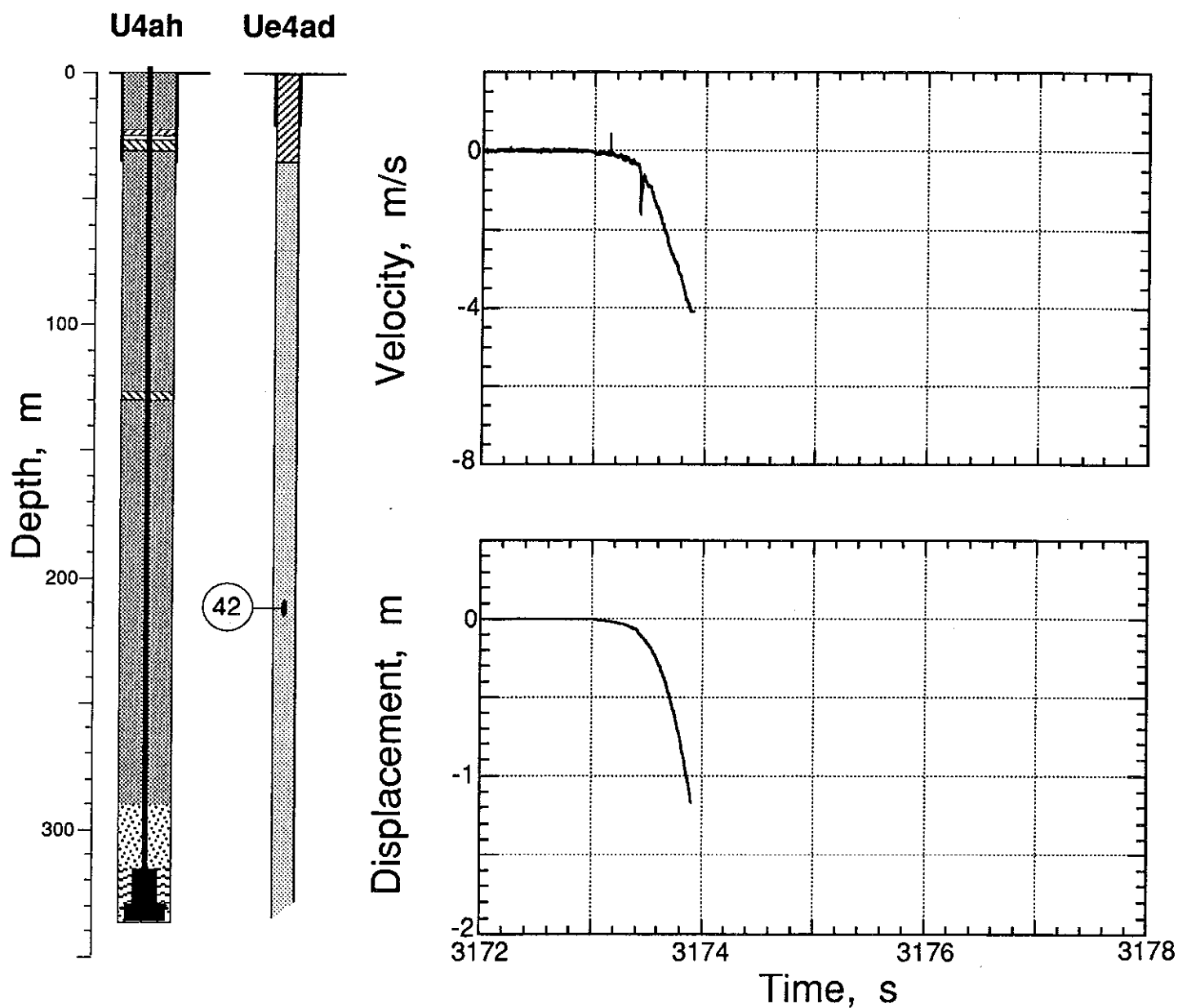


Figure 3.6 Collapse-induced vertical motion of station 42 in the satellite hole (at a depth of 211.5 m).

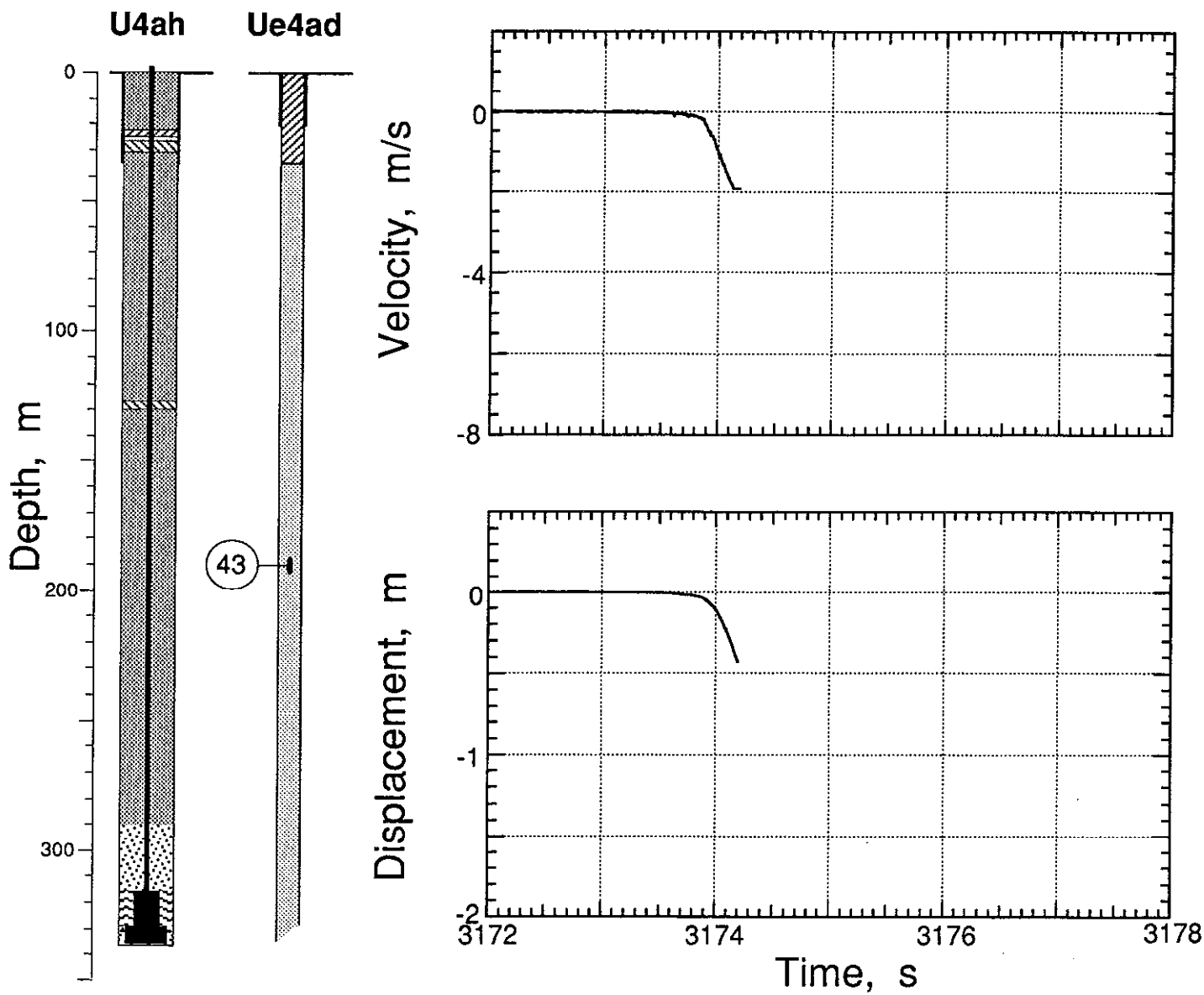


Figure 3.7 Collapse-induced vertical motion of station 43 in the satellite hole (at a depth of 190.2 m).

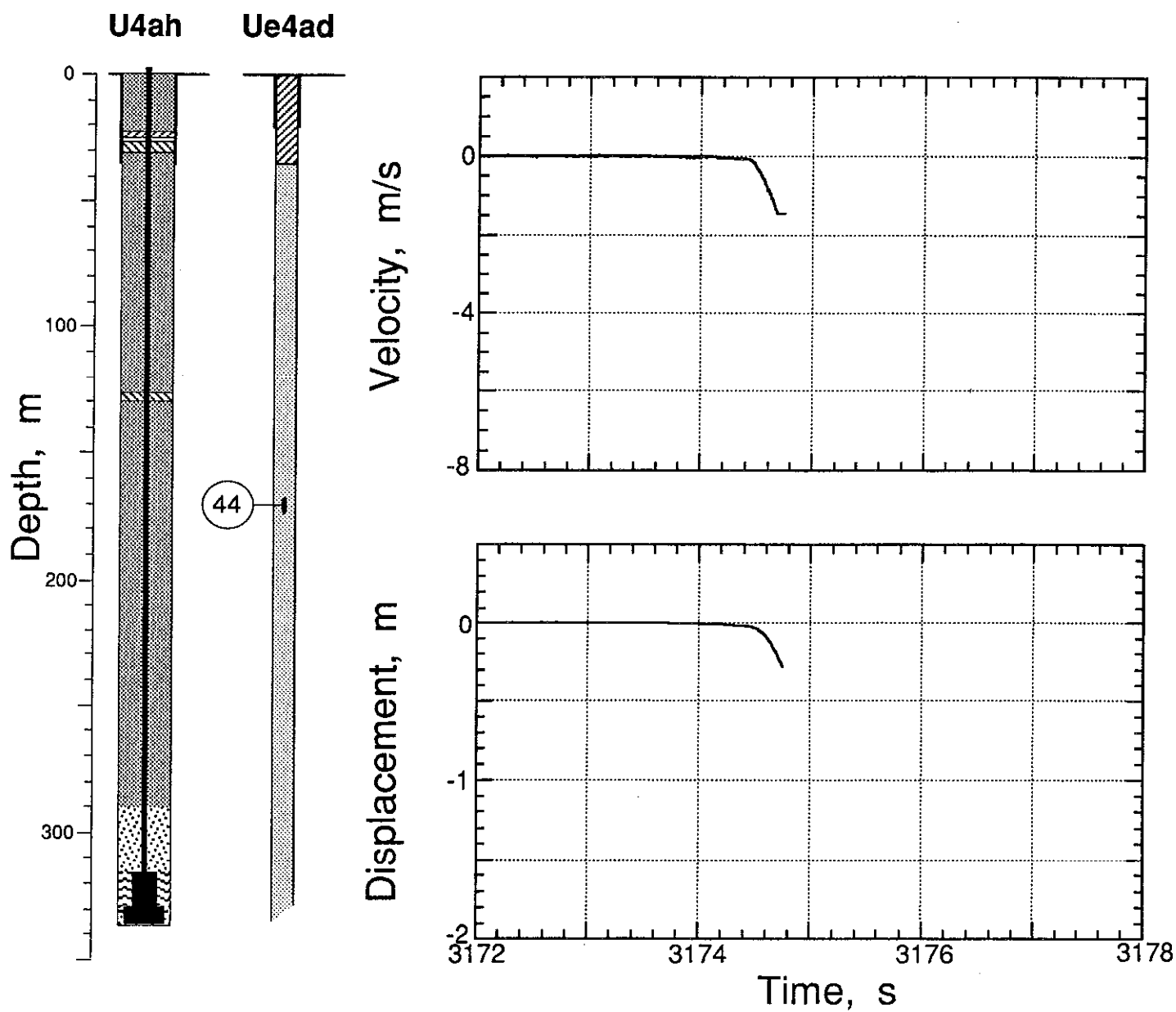


Figure 3.8 Collapse-induced vertical motion of station 44 in the satellite hole (at a depth of 170.3 m).

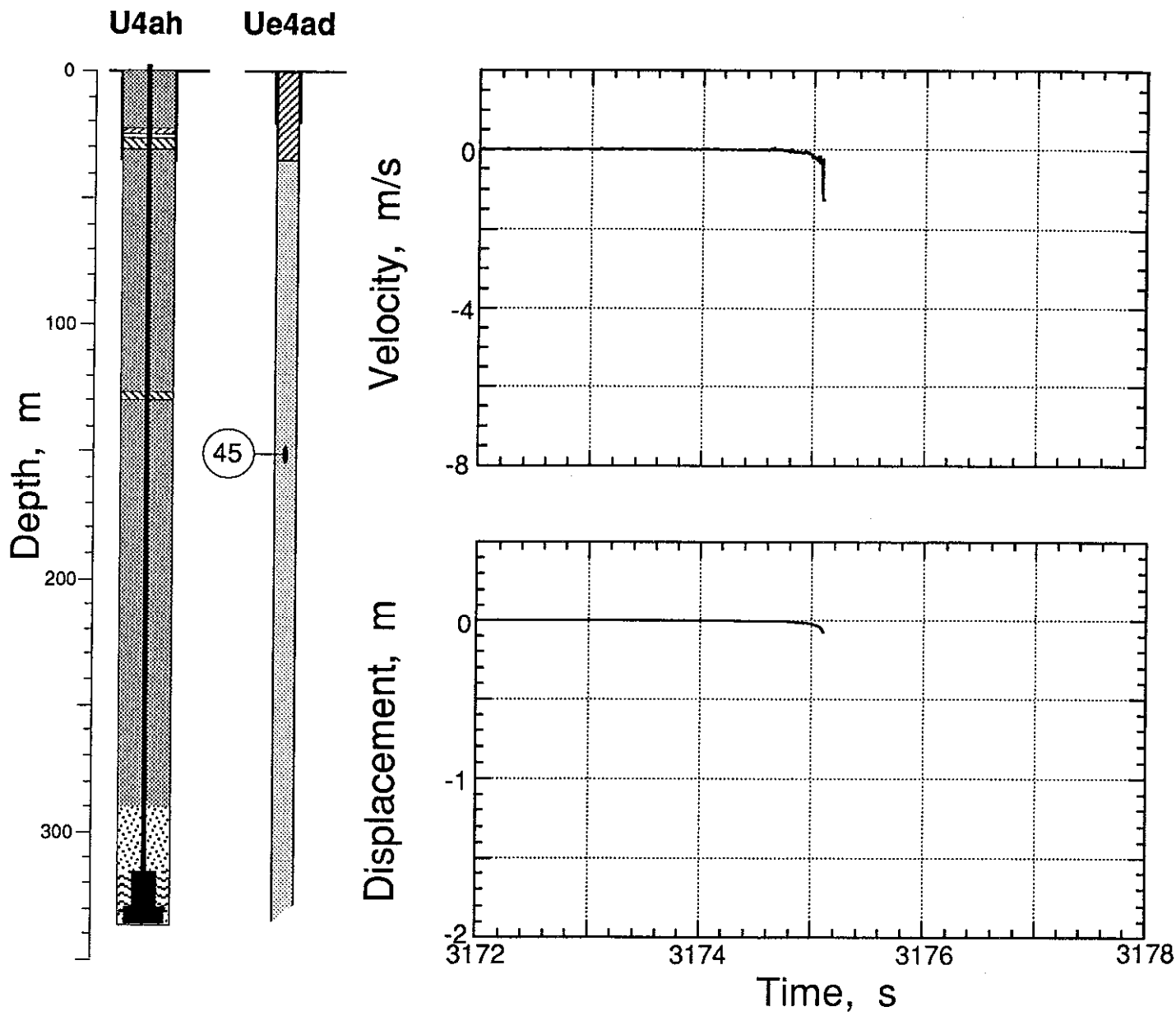


Figure 3.9 Collapse-induced vertical motion of station 45 in the satellite hole (at a depth of 150.4 m).

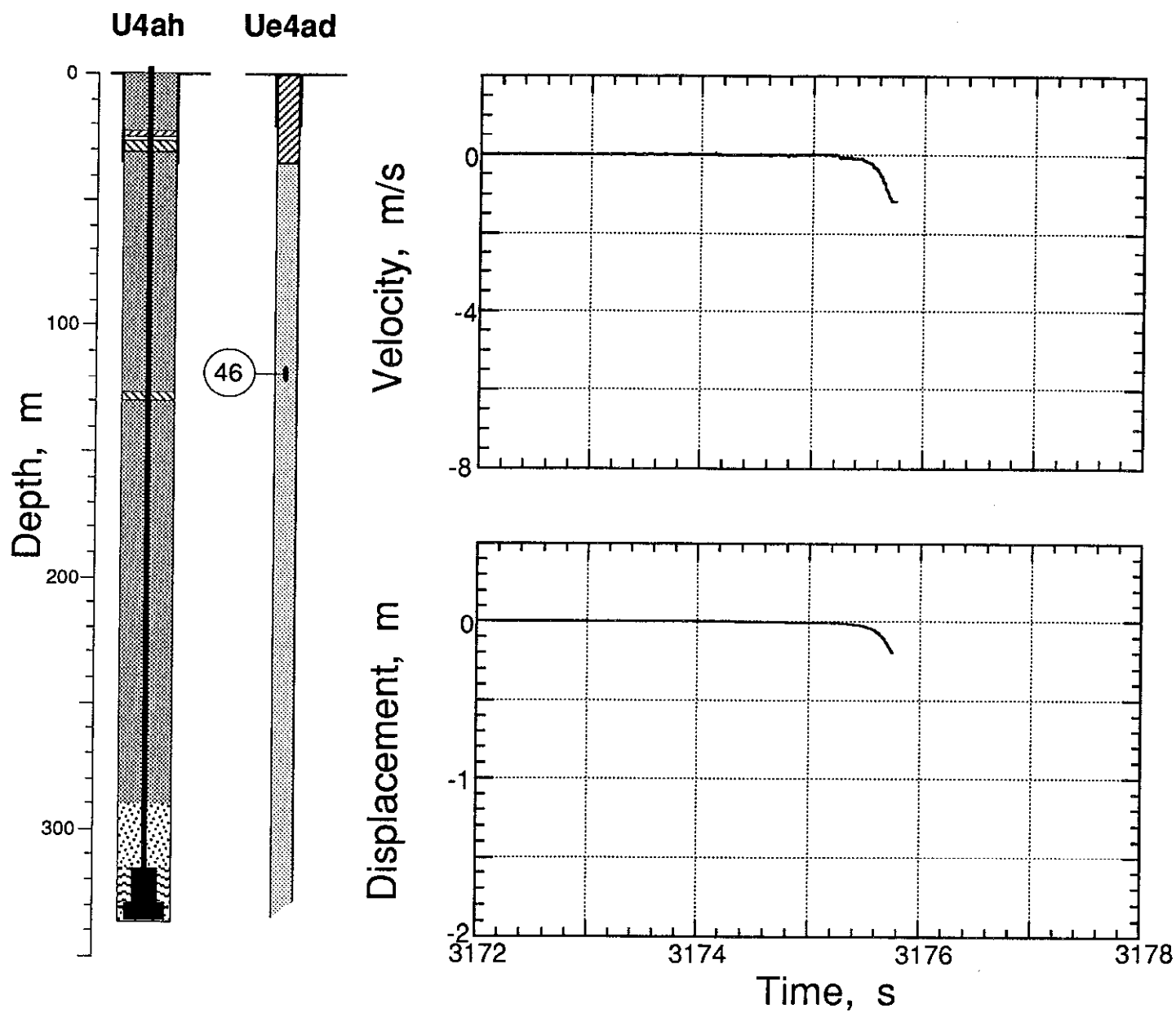


Figure 3.10 Collapse-induced vertical motion of station 46 in the satellite hole (a depth of 119.1 m).

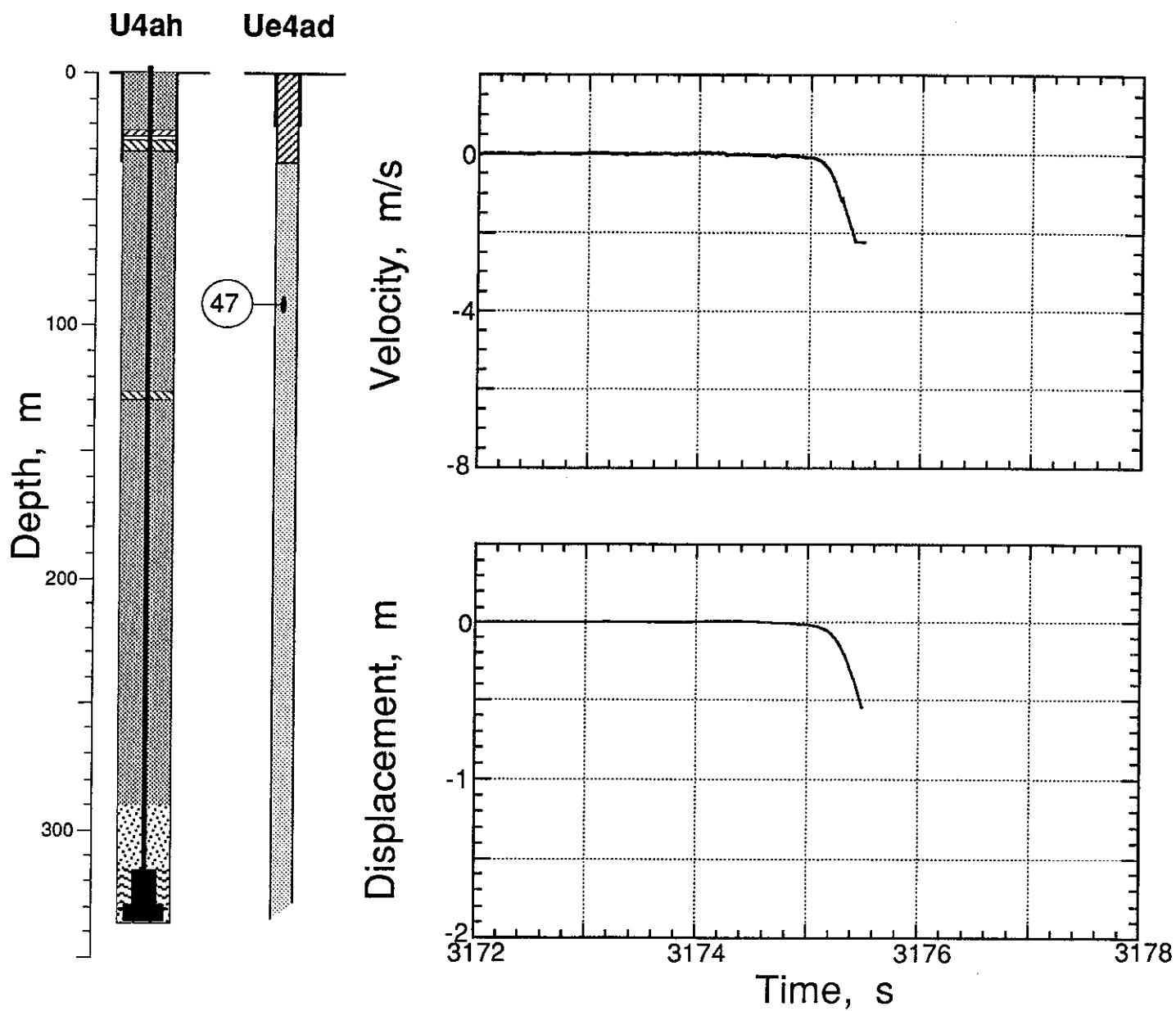


Figure 3.11 Collapse-induced vertical motion of station 47 in the satellite hole (at a depth of 90.8 m).

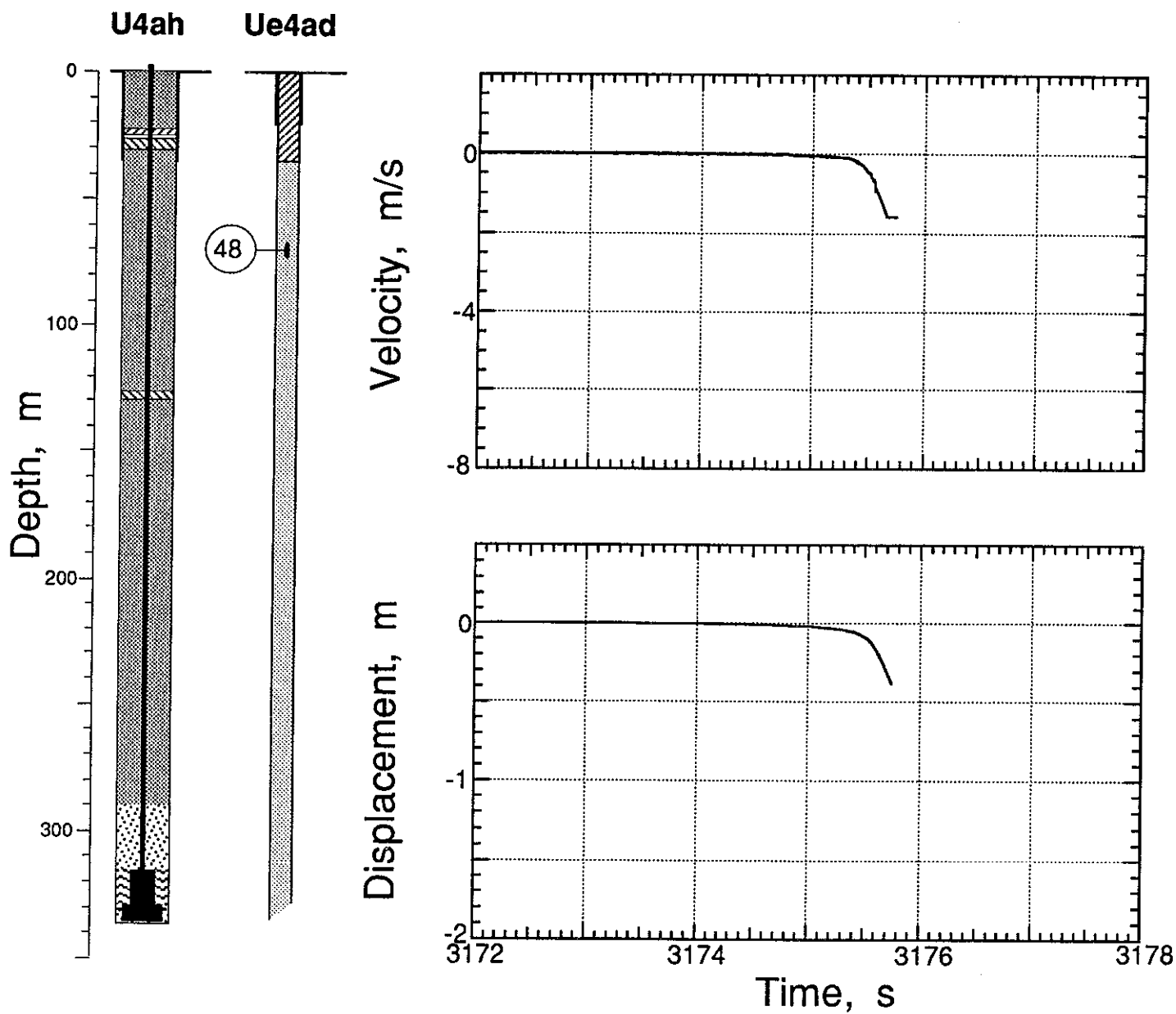


Figure 3.12 Collapse-induced vertical motion of station 48 in the satellite hole (at a depth of 70.0 m).

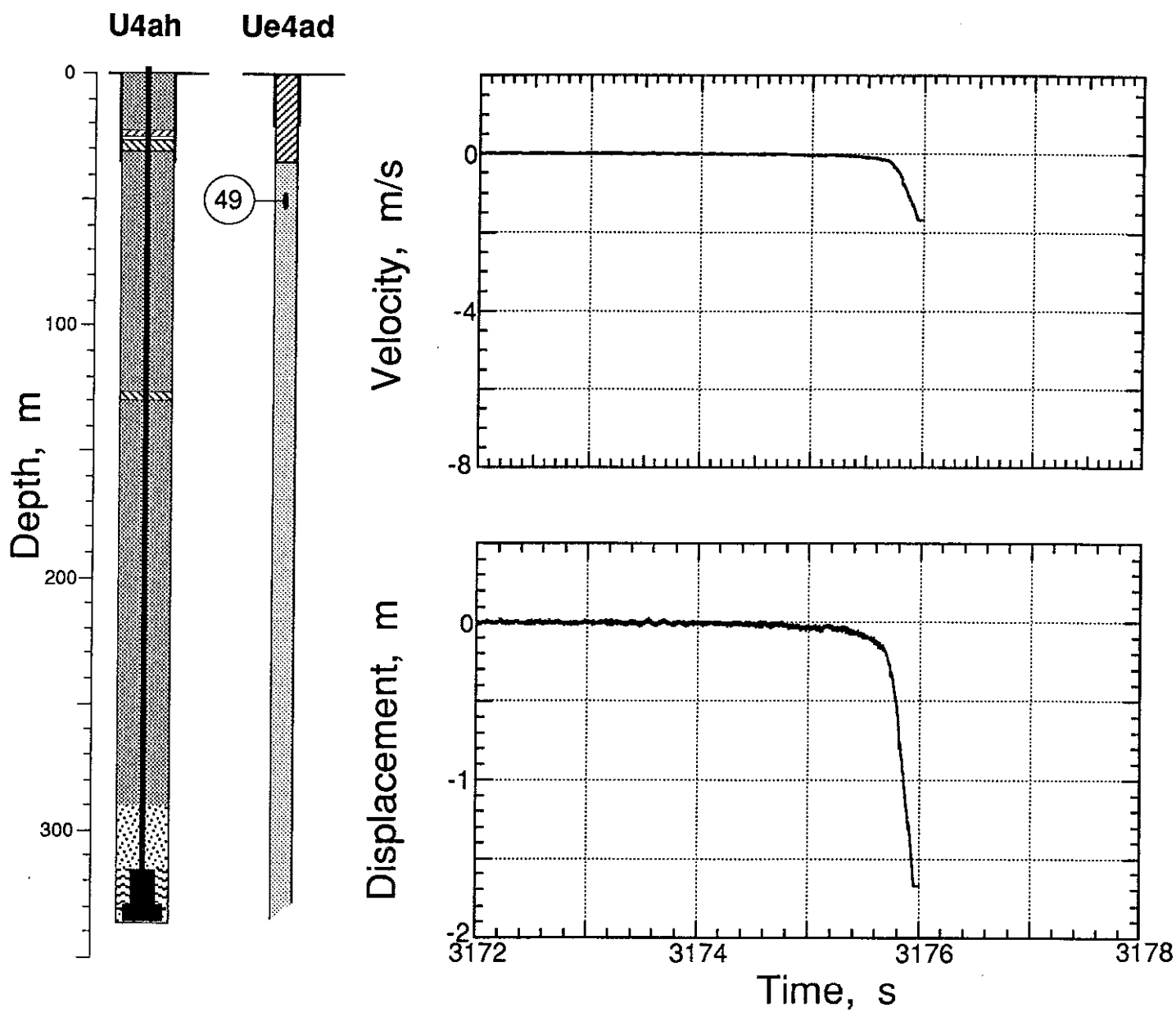


Figure 3.13 Collapse-induced vertical motion of station 49 in the satellite hole (at a depth of 50.2 m).

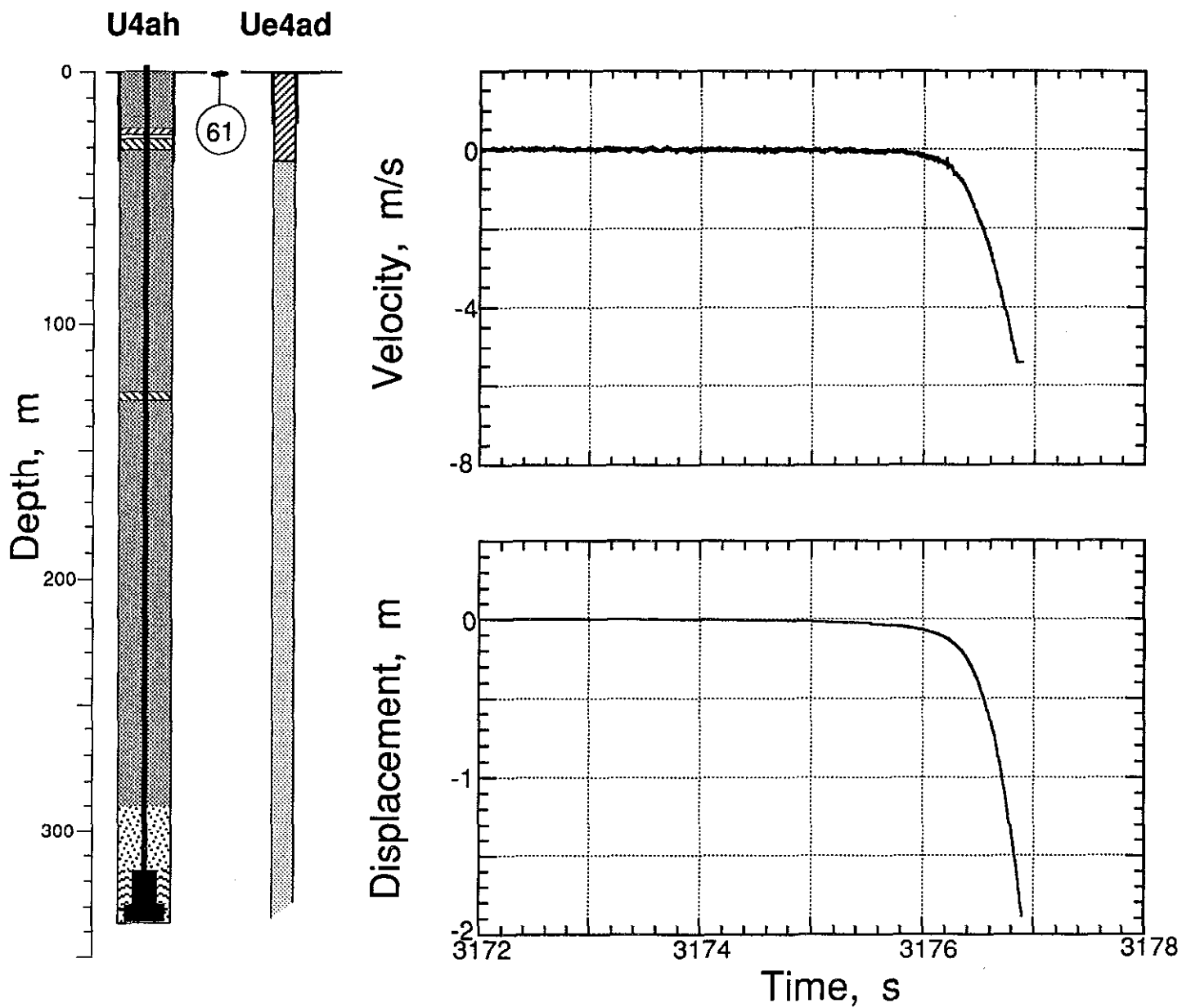


Figure 3.14 Collapse-induced vertical motion of station 61 in the ground surface at a horizontal range of 18.3 m from SGZ and a depth of 1.2 m.

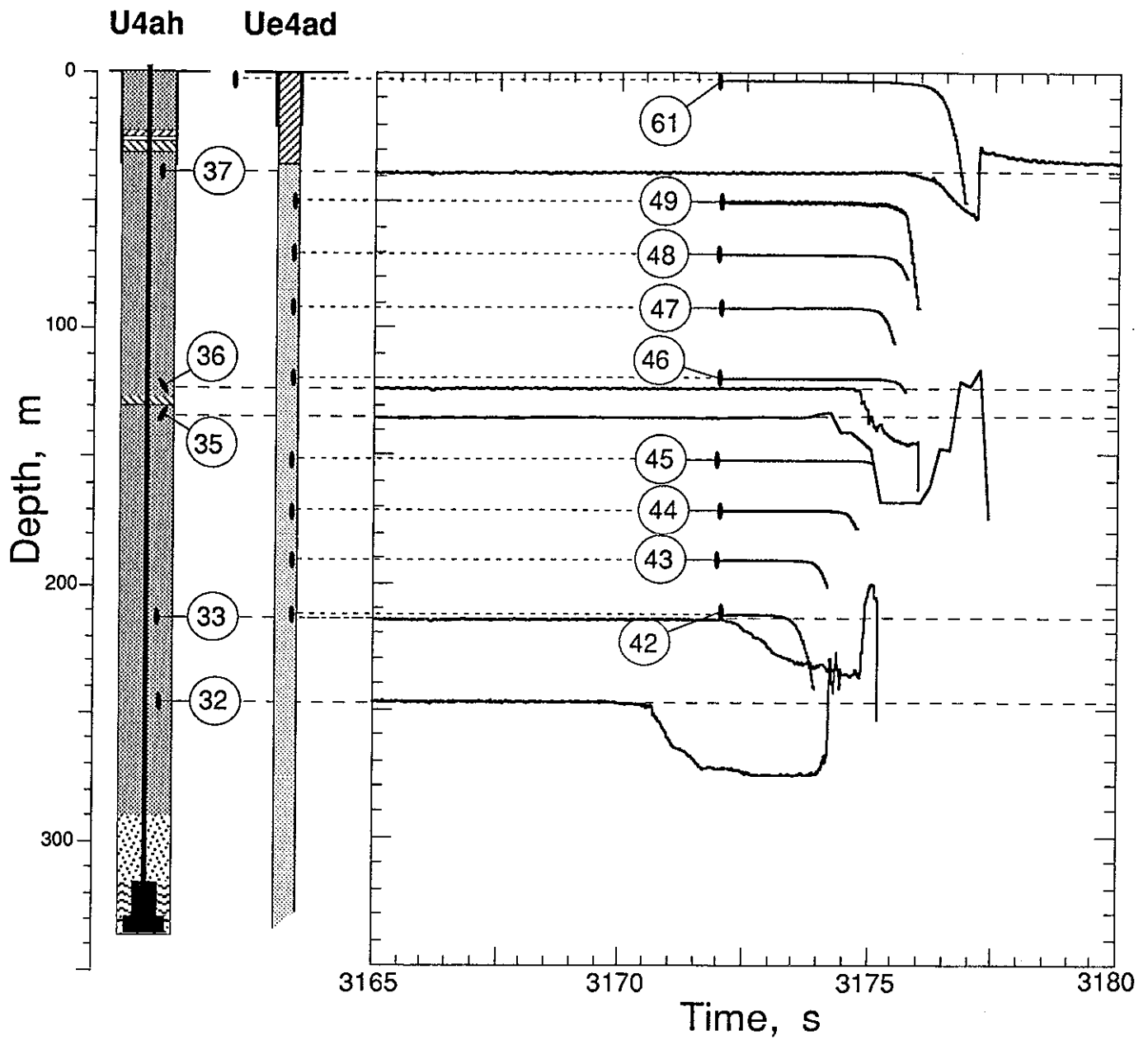


Figure 3.15 Progression of the collapse as indicated by pressure records obtained from the emplacement hole and the displacement records from the satellite hole.

References

1. N. W. Howard, "U4ah Preliminary Site Characteristics Summary ", AGTG 77-102, Lawrence Livermore National Laboratory, Livermore, CA, November 10, 1977.
2. George Kronsbein for William J. Mayer, "Containment Report for U4ah," Holmes & Narver, NTS:A2:79-76, March 15, 1978.
3. William G. Webb, "Special Measurements Physics/Instrumentation Plan for KARAB, Revision 'A' Final", EG&G, Energy Measurements, Las Vegas, NV, SM:79E-72-24, 29 October, 1979.
4. T. Stubbs, R. Heinle, "NORBO Containment Data Report", UCRL-ID- 123238, Lawrence Livermore National Laboratory, Livermore, CA, November, 1995. and T. Stubbs, R. Heinle, "TILCI Containment Data Report", UCRL-ID- 127717, Lawrence Livermore National Laboratory, Livermore, CA, June, 1997.

Distribution:

LLNL

TID/Brenda Staley (3)	L-053
Test Program Library	L-160
Containment Vault	L-221
Burkhard, N.	L-221
Cooper, W.	L-149
Denny, M.	L-205
Goldwire, H.	L-221
Heinle, R. (5)	L-221
Moran, M. T.	L-777
Moss, W.	L-200
Pawloski, G.	L-221
Rambo, J.	L-200
Valk, T.	L-154

LANL

Brunish, W.	F-659
Kunkle, T.	F-665
Trent, B.	F-664

Sandia

Bergstresser, T.	MS-1168
------------------	---------

BNL/AVO

Brown, T.	A-5
Still, G.	A-5
Stubbs, T.	A-5

BNL/NVO

Bellow, B.	N 13-20
Davies, L.	N 13-20
Moeller, A.	N 13-20
Robinson, R.	N 13-20

Defense Special Weapons Agency

Ristvet, B.

Maxwell Technologies

Peterson, E.

Eastman Cherrington Environment

Keller, C.

